MODELLING OF POLLUTANTS IN COMPLEX ENVIRONMENTAL SYSTEMS

Volume I

ADVANCED TOPICS IN ENVIRONMENTAL SCIENCE SERIES

SERIES EDITOR
Grady Hanrahan
John Stauffer Endowed Chair of Analytical Chemistry
California Lutheran University
Thousand Oaks, California, USA

This series of high-level reference works provides a comprehensive look at key subjects in the field of environmental science. The aim is to describe cutting-edge topics covering the full spectrum of physical, chemical, biological and sociological aspects of this important discipline. Each book is a vital technical resource for scientists and researchers in academia, industry and government-related bodies who have an interest in the environment and its future sustainability.

Published titles

Modelling of Pollutants in Complex Environmental Systems, Volume I
Edited by Grady Hanrahan

Forthcoming titles

Modelling of Pollutants in Complex Environmental Systems, Volume II
Edited by Grady Hanrahan

MODELLING OF POLLUTANTS IN COMPLEX ENVIRONMENTAL SYSTEMS

Volume I

Edited by
Grady Hanrahan

Published in 2009 by ILM Publications

Oak Court Business Centre, Sandridge Park, Porters Wood
St Albans, Hertfordshire, AL3 6PH, UK

6635 West Happy Valley Road, Suite 104, #505,
Glendale, AZ 85310, USA

www.ilmpublications.com/www.ilmbookstore.com

British Library Cataloguing in Publication Data

A catalogue record for this book is available from the British Library

Library of Congress Control Number: 2009922569

ISBN 978-1-906799-00-7

Typeset by Keytec Typesetting Ltd, Dorset, UK
Printed and bound in the UK by MPG Biddles Ltd
Cover design by Paul Russen

For orders, visit ILM Bookstore at www.ilmbookstore.com or email sales@ilmbookstore.com

PART III

Subsurface Modelling and Pollutant Transport in Soils

CHAPTER 5

Pollutant Fate and Transport in the Subsurface

Laurin Wissmeier, Alessandro Brovelli, Clare Robinson, Frank Stagnitti and D.A. Barry

5.1 INTRODUCTION

Soil is one of the prime elements that sustain life on earth. Motivated by the desire to increase food production, for millennia humans have modified the landscape by the use of irrigation, drainage and fertiliser application. The soil has also been widely used as a dumping ground for waste. In highly populated regions of the world human modification of the landscape has led to severe deterioration of the soil environment. A better understanding of the myriad complex physical, biological and chemical processes that occur in soil is required to better manage this valuable resource. Mathematical modelling is an important tool, leading to better understanding of the fate of pollutants in the environment.

This chapter considers the fate and transport of pollutants in the subsurface. Figure 5.1 shows, schematically, three major zones through which water flows and biogeochemical reactions occur:

- Surface or near-surface contaminant releases pass through the vadose (unsaturated) zone, in which both air and water are generally present in the soil's pore space. Owing to the presence of air in this zone, the water phase is usually oxygenated, leading to aerobic conditions that support relatively rapid biological activity. Flow tends to be vertically downwards, and can be modelled as a one-dimensional flow problem, with associated reactions. Modelling of this zone is presented in Section 5.2.
- Groundwater flow and transport have a major impact on water supply in many parts of the world. Flow in this zone is approximately horizontal, occurring mainly in the more permeable soil layers. Dissolved oxygen that may be present in recharge water arriving from the vadose zone is depleted rapidly by biological

Modelling of Pollutants in Complex Environmental Systems, Volume I, edited by Grady Hanrahan.

Figure 5.1: Main subsurface zones – unsaturated zone, groundwater aquifer and coastal aquifer – as characterised by different flow dynamics and aerobic/anaerobic status.

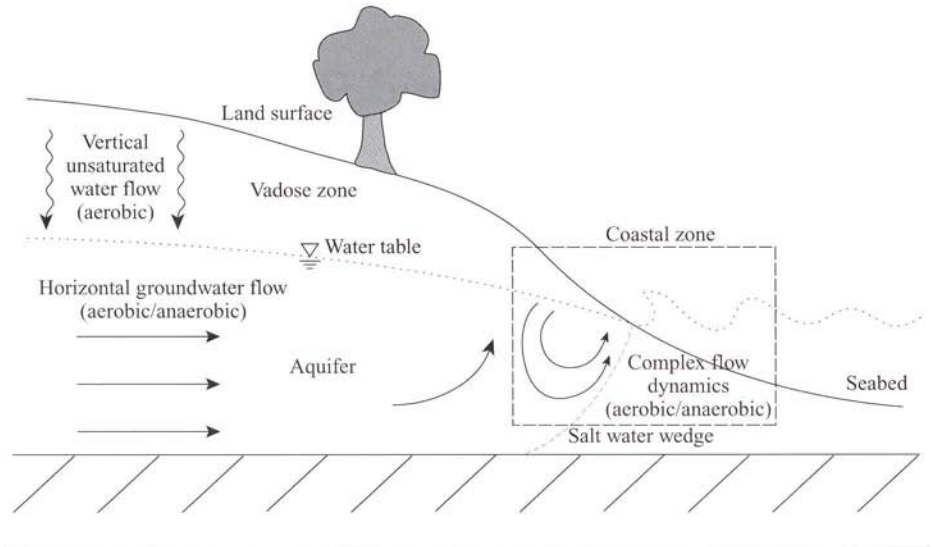

processes, in which case anaerobic microbial communities are the drivers of (relatively slow) biological transformations of contaminants. See Section 5.3 for details.

- In coastal regions, flow patterns are complicated by groundwater discharge to coastal seas, the density differences between groundwater and seawater, and dynamically varying tide and wave conditions. These factors lead to complex, time-dependent flow patterns in the nearshore subsurface region, which in turn impact on contaminant fate and transport, as described in Section 5.4.

This chapter follows the structure outlined above and, as indicated, considers these three regions in detail. Solute transport and reactions in the unsaturated zone above the water table are considered first. A general theoretical framework for the transport and reaction of aqueous species in partially saturated porous media is established. Using this framework, a generic tool for modelling one-dimensional vertical flow and reactive solute transport is presented, and illustrated with examples including kinetic mineral reactions, cation exchange in transient infiltration, and surface adsorption onto variably charged solids.

In groundwater, environmental engineering schemes to enhance biological and inorganic geochemical reactions can modify the physical structure of the soil. These lead to changes in the aquifer's hydraulic properties and thus in the transport paths of solutes and water. Microbial enhancement can lead to obstructions within the porous medium, referred to as *pore clogging* or *bio-clogging*. Pore clogging has many adverse environmental effects and, notably, can lead to ineffective pollution remediation strategies. The physical mechanisms of pore clogging are discussed, and a model of

pore clogging in saturated porous material is presented. The model is illustrated with two examples. The first considers one-dimensional pore clogging, which may be encountered in laboratory column experiments used to characterise natural aquifers. The second example simulates two-dimensional clogging, which has been encountered in passive engineered bioreactive barriers, the latter being a common remediation method.

Discharge of groundwater to coastal seas, commonly referred to as *submarine groundwater discharge* (SGD), has in recent years been identified as an important source of pollution in coastal regions. The chapter concludes with an examination of the fate of pollutants in coastal groundwater. The geochemical processes operative within nearshore aquifers, and which therefore influence the contaminant loadings associated with SGD, are introduced in a conceptual framework. The framework is used to discuss the influence of tides on groundwater flow and transport of recirculating seawater in the nearshore subsurface region. The implications for transport and reaction of contaminants in the coastal zone are also discussed and illustrated.

5.2 SOLUTE TRANSPORT AND REACTIONS IN THE UNSATURATED ZONE

5.2.1 Mass balance equation

In a multiphase, multi-species system such as a partially water-saturated porous medium, the general mass balance equation can be expressed in three dimensions as (e.g., Miller *et al.*, 1998; Barry *et al.*, 2002):

$$\frac{\partial}{\partial t}(\theta_\alpha \rho_\alpha \omega_{i\alpha}) = -\nabla \cdot (\theta_\alpha \rho_\alpha \omega_{i\alpha} \boldsymbol{v}_\alpha) - \nabla \cdot \boldsymbol{j}_{i\alpha} + \mathcal{J}_{i\alpha} + \mathcal{R}_{i\alpha} + \mathcal{S}_{i\alpha} \qquad (5.1)$$

with time t, volume fraction θ, density ρ ($\mathrm{M\,L^{-3}}$), mass fraction ω, mean pore fluid velocity vector $\boldsymbol{v}$ ($\mathrm{L\,T^{-1}}$), non-advective transport $\boldsymbol{j}$ ($\mathrm{M\,L^{-2}\,T^{-1}}$), interphase mass exchange $\mathcal{J}$ ($\mathrm{M\,L^{-3}\,T^{-1}}$), intraphase reaction $\mathcal{R}$ ($\mathrm{M\,L^{-3}\,T^{-1}}$) and external source $\mathcal{S}$ ($\mathrm{M\,L^{-3}\,T^{-1}}$). Subscripts α denote phases and i species within phases, to all of which Equation 5.1 applies. Thus, for example, the subscript $i\alpha$ refers to the i^{th} species in the α phase, and θ_α is the volume fraction of the α phase (gas, liquid or solid).

Following Miller *et al.* (1998), the identities

$$\sum_\alpha \theta_\alpha = 1, \quad \sum_\alpha \mathcal{J}_{i\alpha} = 0, \quad \sum_i \omega_{i\alpha} = 1, \quad \sum_i \boldsymbol{j}_{i\alpha} = 0, \quad \sum_i \mathcal{R}_{i\alpha} = 0 \qquad (5.2)$$

can be applied to Equation 5.1. In particular, considering a single liquid (aqueous phase) a and an immobile (solid or mineral) phase s, the mass balance for each phase is obtained by summing over all species ia and is:

$$\frac{\partial}{\partial t}(\theta_a \rho_a) = -\nabla \cdot (\theta_a \rho_a \boldsymbol{v}_a) + \sum_i \mathcal{J}_{ia} + \sum_i \mathcal{S}_{ia} \tag{5.3}$$

$$\frac{\partial}{\partial t}(\theta_s \rho_s) = \sum_i \mathcal{J}_{is} + \sum_i \mathcal{S}_{is} \tag{5.4}$$

In Equation 5.3, θ_a is the volumetric moisture content of the aqueous phase and θ_s is the volumetric content of the solid phase. If there are no external sources, then $\sum_i \mathcal{J}_{ia} = -\sum_i \mathcal{J}_{is}$ and Equations 5.3 and 5.4 can be combined to yield

$$\frac{\partial}{\partial t}(\theta_a \rho_a) = -\nabla \cdot (\theta_a \rho_a \boldsymbol{v}_a) - \frac{\partial}{\partial t}(\theta_s \rho_s) \tag{5.5}$$

As can be seen from Equation 5.5, mineral reactions (final term in the equation) affect the flow directly by changing phase saturation. They also act indirectly by altering constitutive relations.

5.2.2 Momentum balance: flow equation for the aqueous phase

The volume flux $\boldsymbol{q}_a$ of the aqueous phase a is given by Darcy's law (e.g., Barry *et al.*, 2002):

$$\theta_a \boldsymbol{v}_a = \boldsymbol{q}_a = -\frac{\boldsymbol{k}_a}{\mu_a} \cdot (\nabla p_a + \rho_a \nabla z) \tag{5.6}$$

where $\boldsymbol{k}_a$ (L^2) is the effective permeability tensor, μ_a ($\mathrm{M\,L^{-1}\,T^{-1}}$) is the dynamic viscosity, p_a ($\mathrm{M\,L^{-1}\,T^{-2}}$) is the fluid pressure, and z (L) is the downward distance from the soil surface.

5.2.3 Transport equations

Species transport (for each species i) in the aqueous phase a evolves according to the general transport equation

$$\frac{\partial}{\partial t}(\theta_a C_{ia}) = -\nabla \cdot (\theta_a \boldsymbol{v}_a C_{ia}) - \nabla \cdot \boldsymbol{j}_{ia} + \mathcal{J}_{ia} + \mathcal{R}_{ia} + \mathcal{S}_{ia} \tag{5.7}$$

with the non-advective transport vector $\boldsymbol{j}$ ($\mathrm{M\,L^{-2}\,T^{-1}}$) and species concentration C ($\mathrm{M\,L^{-3}}$). Using the standard hydrodynamic dispersion for non-advective transport, $\boldsymbol{j}$ can be expressed as

$$\boldsymbol{j}_{ia} = \theta_a \boldsymbol{D}_{ia} \cdot \nabla C_{ia} \tag{5.8}$$

where $\boldsymbol{D}$ is the hydrodynamic dispersion coefficient tensor ($\mathrm{L^2\,T^{-1}}$). Hydrodynamic dispersion can be further split into longitudinal dispersivity d_l (L), transversal dispersivity d_t (L) and effective molecular diffusivity $D_{i\,\mathrm{eff}}$ ($\mathrm{L^2\,T^{-1}}$) according to

$$(D_{ia})_{ij} = \delta_{ij} d_l |v| + (d_l - d_t) \frac{v_i v_j}{|v|} + \delta_{ij} D_{i\,\mathrm{eff}} \tag{5.9}$$

In Equation 5.9, which employs the summation convention, δ is the Kronecker delta function.

5.2.4 Reactions

Reactions can be divided into the two categories of homogeneous reactions within the liquid phase (solution speciation $\mathcal{R}$), and interphase mass exchange between the liquid and the solid phase ($\mathcal{J}$). Since adsorbed ions are immobile, their association with adsorption sites is counted as a heterogeneous reaction.

In the framework of geochemical modelling, species can be represented by a minimum number of master species or components in a linearly independent set of mass action equations (e.g., Lichtner, 1985, 1997).

Table 5.1 illustrates the hierarchy of master species, which form species through association and speciation reactions, and then belong to either the liquid or the solid phase. Mass action equations for different species classes are provided in the following.

Solution speciation

The mass action equation for aqueous species is

$$K_{ia} = \mathcal{A}_{ia} \prod_e \mathcal{A}_e^{-c_{e,ia}} \tag{5.10}$$

with the equilibrium constant K_{ia}, activities $\mathcal{A}$ and stoichiometric coefficient c. Activities of aqueous and master species are defined by

$$\mathcal{A}_n = \gamma_n m_n \quad n = ia, e \tag{5.11}$$

where m_n is the molality of species n, with activity coefficient γ_n (kg water mol^{-1}), which is commonly calculated by the Davies equation, the extended Debye–Hückel equation (Truesdell and Jones, 1974) or the Pitzer model (Pitzer, 1979).

Table 5.1: Relation between master species ***e***, species ***i*** and phases ***α***. The master species are often elements (left column). These combine into (or appear directly as) species, which are found in solution or in the solid (mineral) phases (middle column). The species, taken together, form the solid and fluid phases (right column).

Master species e including exchange and adsorption sites	Solution species $i\alpha$	→ Mobile aqueous phase α
	Exchange species ix	→ Immobile solid phase s
	Surface species iy	→ Immobile solid phase s
	Equilibrium phases im	→ Immobile solid phase s
	Kinetic phases ik	→ Immobile solid phase s

From Equation 5.10 the moles of aqueous species in the system, n_{ia}, can be calculated according to

$$n_{ia} = m_{ia} W_{\text{aq}} = \frac{K_{ia} W_{\text{aq}}}{\gamma_{ia}} \prod_e \mathcal{A}_e^{c_{e,ia}} \tag{5.12}$$

with the mass of water in the aqueous phase W_{aq}.

Equilibrium mineral reactions

For pure mineral phases the mass action equation becomes

$$K_{im} = \prod_e \mathcal{A}_e^{c_{e,im}} \tag{5.13}$$

since the activity of a pure phase is always unity with the common thermodynamic definition of the standard state. The number of moles of mineral is calculated by stoichiometric adjustment of ion concentration in solution according to the target saturation index (SI):

$$\text{SI} = \log_{10}\left(\prod_e \mathcal{A}_e^{c_{e,m}}\right) \tag{5.14}$$

Equilibrium cation exchange reaction

The mass action equation for cation exchange reactions is given by

$$K_{im} = \mathcal{A}_{ix} \prod_e \mathcal{A}_e^{-c_{e,ix}} \tag{5.15}$$

with moles of immobile exchange species

$$n_{ix} = \frac{K_{ix}}{\gamma_{ix}} \frac{T_x}{b_{ix}} \prod_e \mathcal{A}_e^{c_{e,ix}} \tag{5.16}$$

Here, b_{ix} is the number of exchange sites occupied by exchange species ix, and T_x is the total number of equivalents of exchange sites. For the definition of the standard state of exchange species, where the activity is unity, several conventions can be employed (Appelo and Postma, 2005). The most common conventions are mole fractions (Vanselow, 1932), fraction of number of exchange sites (Gapon, 1933), or equivalent fractions (Gaines and Thomas, 1953).

Equilibrium surface adsorption on variable charge surfaces with a diffuse double layer

A basic theory for surface complexation reactions and associated effects of electrostatic potentials was presented by Davis and Kent (1990) and Dzombak and Morel (1990). Following the diffuse double layer model (Dzombak and Morel, 1990), the mass action equation for the adsorption of ions onto variable-charge surface sites is expressed as

$$K_{iy}^{\text{int}} = \left(\mathcal{A}_{iy} \prod_e \mathcal{A}_e^{-c_{e,iy}} \right) \exp\left(\frac{F\Psi}{RT} \Delta z_{iy} \right) \tag{5.17}$$

where the intrinsic equilibrium constant K^{int} is modified by an exponential electrostatic term with the Faraday constant F (C mol^{-1}), surface potential Ψ (V), gas constant R (J mol^{-1} K^{-1}) and net change in surface charge due to the formation of the surface species Δz_{iy}. The moles of immobile surface species can be calculated from (Parkhurst and Appelo, 1999)

$$n_{iy} = K_{iy}^{\text{int}} T_y \exp\left(-\frac{F\Psi}{RT} \Delta z_{iy} \right) \prod_e \mathcal{A}_e^{c_{e,iy}}, \tag{5.18}$$

with T_y being the total number of equivalents of surface sites.

Other surface complexation models have been published in the literature (e.g., Hiemstra and Van Riemsdijk, 1996, 1999; Rietra *et al.*, 1999). Since they are usually more complicated and numerically involved, their applicability to large-scale problems in environmental engineering is limited.

Kinetic mineral and gas-phase reactions

All of the above reactions employ the mass action equation and therefore assume local equilibrium. However, if the timescale of transport is in the range of the timescale of reaction, the dynamics of the reaction process have to be considered. Because of the many, often non-linear, dependences of reaction rates on geochemical properties, such as saturation indices, ionic strength, temperature and pH, and because of the ongoing increase in knowledge of reaction processes, no universal rate law can be formulated. Thus the most general formulation of kinetic reactions is

$$\frac{\mathrm{d}m_{e,ik}}{\mathrm{d}t} = c_{e,ik} R_k \tag{5.19}$$

where the change of master species m_e (mol) with time is given by a reactant specific rate R_k (mol T^{-1}) and the stoichiometry $c_{e,ik}$ of the charge-balanced kinetic reactant ik.

5.2.5 Numerical model implementation

In this section we present a generic tool for one-dimensional flow, solute transport and reaction in the vadose zone. The governing equations (outlined above) are solved by implementing a numerical solution of the moisture-based form of Richard's equation in the geochemical modelling framework PHREEQC (Parkhurst and Appelo, 1999). Direct integration of the flow and transport into the unmodified PHREEQC source code, without coupling to other software, provides access to the entire set of geochemical reactions and databases that are currently implemented in PHREEQC, and also ensures compatibility with future versions.

Split operator

A split operator approach is employed for the decoupling of simultaneous processes of Darcian flow, element transport and geochemical reactions in a discretised time domain. Key references on operator-splitting techniques and their performance are Yeh and Tripathi (1989, 1991), Mangold and Tsang (1991), Steefel and Lasaga (1994), Barry *et al.* (1996a, 1996b, 1997, 2000) and Kanney *et al.* (2003). Here we present a numerical scheme built on a sequential split-operator scheme. This method provides first-order accuracy in the time discretisation, $O(\Delta t)$, and is consistent with the accuracy of the explicit finite difference scheme used for Richards' equation (outlined in the next section). Owing to the separate treatment of reactions, their contribution to flow and solute transport are not taken into account in the following equations. Rather, they are modelled as a subsequent step in the split-operator scheme. Since only flow as a single liquid phase is considered, we redefine $\theta_a = \theta$.

Moisture-based flow

Upon simplifying Equation 5.6 for one-dimensional vertical flow of a single incompressible aqueous phase with constant density, the Darcy flux can be written as

$$q = K(\theta) - D(\theta)\frac{\partial \theta}{\partial z} \tag{5.20}$$

where K (LT^{-1}) is the hydraulic conductivity, and θ and q are now the aqueous water content and Darcy velocity (LT^{-1}), respectively. The moisture capillary diffusivity D ($\mathrm{L}^2\mathrm{T}$) is defined as

$$D(\theta) \equiv K(\theta)\frac{\mathrm{d}h}{\mathrm{d}\theta} \tag{5.21}$$

where h (L) is the hydraulic head. Combining Equations 5.3 and 5.20 leads to the moisture-based form of Richards' equation (e.g., Klute, 1952; Philip, 1969; Celia *et al.*, 1990):

$$\frac{\partial \theta}{\partial t} = \frac{\partial}{\partial z}\left[D(\theta)\frac{\partial \theta}{\partial t}\right] - \frac{\partial K(\theta)}{\partial z} \tag{5.22}$$

Kirchhoff transformation of the diffusivity term

Tocci *et al.* (1997) noted that variable transformation methods in the numerical solution of Richards' equation can reduce computational costs significantly. Transformations have been successfully applied (Ross, 1990; Ross and Bristow, 1990; Kirkland *et al.*, 1992; Miller and Kelley, 1994). Here, the Kirchhoff transformation (e.g., Philip, 1989; Pullan, 1990; Raats, 2001) is applied to the diffusivity term in Equation 5.23:

$$J(\theta) = \int_{\theta_{\mathrm{res}}}^{\theta} D(\theta)\mathrm{d}\theta \tag{5.23}$$

with J ($\mathrm{L}^2\mathrm{T}$) being the integrated diffusivity and θ_{res} the residual water content.

Because of this transformation, Equation 5.23 can be rewritten in the form of an advection–dispersion equation:

$$\frac{\partial \theta}{\partial t} = \frac{\partial^2 J(\theta)}{\partial z^2} - \frac{\partial K(\theta)}{\partial z} \tag{5.24}$$

Element transport

With the definition of chemical elements E as master species and species-independent non-advective transport, the solute transport equation becomes

$$\frac{\partial}{\partial t}(\theta[E^e]) = -\frac{\partial}{\partial z}(q[E^e]) - D^{\mathrm{h}} \frac{\partial}{\partial z}\left(\theta \frac{\partial [E^e]}{\partial z}\right) \tag{5.25}$$

where D^{h} ($\mathrm{L^2\,T^{-1}}$) is the (assumed constant) hydrodynamic dispersion coefficient, and square brackets denote molar concentrations.

Traditionally, solute transport is calculated for selected solution species in the aqueous phase only. However, it is recognised that Equation 5.25 solves Richards' equation if it is applied to all aqueous elements and divided by the aqueous phase density, since the net non-advective transport is zero according to Equation 5.2:

$$\frac{\partial \theta}{\partial t} = -\sum_e \frac{\partial}{\partial z}\left(\frac{\varepsilon^e [E^e] q}{\rho}\right) \tag{5.26}$$

Then, water flow results from transport of oxygen and hydrogen, which are treated like any other element in the aqueous phase. In Equation 5.26, ε is the molar element mass ($\mathrm{M\,mol^{-1}}$).

Finite-difference scheme

An explicit, upwind finite-difference scheme is applied to the element transport equation according to

$$\frac{\theta_i^{n+1}[E^e]_i^{n+1} - \theta_i^n [E^e]_i^n}{\Delta t} = \frac{q^n_{i-\frac{1}{2}}[E^e]^n_{i-1} - q^n_{i+\frac{1}{2}}[E^e]^n_i}{\Delta z} \tag{5.27}$$

where subscript i is here taken as the index of the current cell, and $i-1$ is the index of the upstream cell (such that flow occurs between $i-1$ and i). Current and future time steps are indicated by superscripts n and $n+1$, respectively. Hydrodynamic dispersion is generated through numerical dispersion, which is introduced by the first-order space discretisation.

With the upstream boundary flux $q_{i-\frac{1}{2}}$ computed as

$$q_{i-\frac{1}{2}} = \frac{J_{i-1} - J_i}{\Delta z} - \frac{K_{i-1} + K_i}{2} \tag{5.28}$$

and the downstream flux calculated analogously, the accuracy of the scheme is $\mathcal{O}(\Delta t, \Delta z)$ for solute concentrations and $\mathcal{O}(\Delta t, \Delta z^2)$ for the aqueous phase saturation.

This scheme was validated for numerous hydraulic properties and boundary conditions, and – primarily because of the Kirchhoff transformation – gives accurate solutions, even with a coarse spatial discretisation (Wissmeier and Barry, 2008).

Constitutive equations

For the following example applications, we use the van Genuchten model (van Genuchten, 1980) for water retention:

$$\Theta = \left[\frac{1}{1 + (\alpha_g h)^{n_g}}\right]^{m_g} \tag{5.29}$$

with reduced water content $\Theta = (\theta - \theta_{res})(\theta_{sat} - \theta_{res})^{-1}$, saturated water content θ_{sat} and van Genuchten parameters α_g (L^{-1}), n_g and $m_g = 1 - n_g^{-1}$. The Mualem model (Mualem, 1976),

$$K(\Theta) = K_{sat}\sqrt{\Theta}\left[1 - (1 - \Theta^{1/m_g})^{m_g}\right]^2 \tag{5.30}$$

with saturated hydraulic conductivity K_{sat} (LT^{-1}) is used to calculate unsaturated hydraulic conductivity. The analytical integration of the moisture diffusivity function according to the van Genuchten model, Equation 5.23 results in hypergeometric functions, which are evaluated numerically using algorithms from Spanier and Oldham (1987).

5.2.6 Example applications

The following examples illustrate three applications of the generic model to environmentally relevant geochemical processes in transient unsaturated flow conditions. Although the model described here is capable of simulating a multitude of simultaneous geochemical reactions, we avoid this in order to facilitate a clear interpretation of the results.

Kinetic mineral reaction

Local equilibrium as applied in reactive transport modelling is predicated on the assumption that the kinetics of geochemical processes are fast enough for them to be treated as instantaneous. In practice, this means that the timescale for flow through a computation cell is much larger than the reaction timescale. However, for a large number of mineral dissolution/precipitation reactions the timescales of flow and reaction coincide, such that their treatment using the local equilibrium assumption leads to erroneous results.

This simulation illustrates the combined effect of infiltration of pure water into a sandy soil and kinetic dissolution of a solid calcite phase. Calcite is dissolving according to the rate equation

$$R_{calcite} = \frac{p_1}{10}\left(\frac{CaCO_3^s}{CaCO_3^{s,0}}\right)^{p_2}\left(k_1\{H^+\} + k_2\{CO_2\} + k_3\{H_2O\}\right)\left(1 - 10^{\frac{2}{3}SI}\right) \tag{5.31}$$

where

$$\log_{10}(k_1) = 0.198 - \frac{444}{273.16 + T_C}$$

$$\log_{10}(k_2) = 2.84 - \frac{2177}{273.16 + T_C}$$

$$\log_{10}(k_3) = \begin{cases} -5.86 - \dfrac{317}{273.16 + T_C} & T_C \leq 25 \\ -1.1 - \dfrac{1737}{273.16 + T_C} & T_C > 25 \end{cases}$$

with actual moles of calcite per litre of soil $CaCO_3^s$, initial moles of calcite per litre of soil $CaCO_3^{s,0}$, parameter $p_1 = 50$, which is related to the ratio of surface area and mineral volume, parameter $p_2 = 0.6$, temperature T_C (°C), and saturation index for calcite SI; k_1, k_2, k_3 and therefore $R_{calcite}$ are in units of mol s^{-1}. In Equation 5.31 braces denote species activities. The rate equation is taken from the standard PHREEQC database (Parkhurst and Appelo, 1999).

A plot of the reaction progress in a batch system with 0.1 mmol of calcite in 1 L of pure water at 20°C is given in Figure 5.2. The half-life after which 50% of the initial calcite is dissolved is 112 s.

The hydraulic properties in the soil column are those of sandy loam (Šimůnek *et al.*, 2005) with $\theta_{sat} = 0.41$, $\theta_{res} = 0.057$, $\alpha_g = 0.124\ mm^{-1}$, $n_g = 2.28$ and

Figure 5.2: Kinetic calcite dissolution.

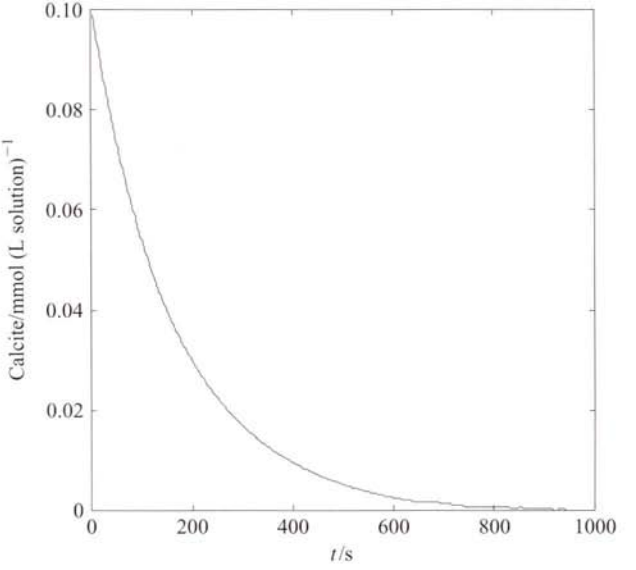

$K_{sat} = 0.243$ mm s^{-1}. The initial solution is saturated with respect to calcite with a surplus of 0.1 mmol of solid calcite per litre of soil. Initial and boundary conditions are

$$\begin{aligned} &t = 0,\ z \geqslant 0,\ \theta = 0.1 && C = c_{ini} \\ &t \geqslant 0,\ z = 0,\ q = 0.01 \text{ mm s}^{-1} && C = 0 \\ &t \geqslant 0,\ z \to \infty,\ \theta = 0.1 && C = c_{ini} \\ &c_{ini}:\ [Ca^{+2}] = 1.227 \times 10^{-4},\ [CO_3^{-2}] = 1.227 \times 10^{-4} \end{aligned} \tag{5.32}$$

where again the brackets denote molar concentrations. The simulation domain was long enough that the infiltration front did not interact with the downstream boundary, so as to satisfy the semi-infinite domain condition in Equation 5.32. A spatial discretisation of 0.1 cm was used, and the transport time step was 0.1 s.

Figure 5.3a shows the progressing infiltration front due to the high permeability of the loamy sand. In this simulation, due to the low flux at the upper boundary, progress of the moisture front is relatively slow and shows strong moisture diffusion.

Calcium concentrations in the solution are displayed in Figure 5.3b. Flushing of calcium by infiltrating fresh water is retarded compared to the moisture front due to continuous dissolution of calcite.

The moles of calcite per litre of soil are shown in Figure 5.3c. In an equilibrium simulation dissolution takes place only in the first cell in the direction of flow, where the mineral is present and the solution is undersaturated. Here the solution is completely saturated, so that no further dissolution takes place downstream. In the case of kinetic mineral reactions the solution does not reach a saturation index of zero after the first contact with the mineral, leaving some dissolution capacity downstream. The slope of the dissolution front is dependent on the reaction rate compared with the flow velocity. For equilibrium there is an abrupt change from the initial amount of the mineral, whereas very slow dissolution reactions affect the mineral uniformly throughout the column. In the presented example, the half-life of the dissolution reaction is on a similar timescale as the infiltration process, which leads to the dispersed dissolution front.

As a result of complete solution speciation, the pH that results from the dissolution reaction can be followed in the simulation (Figure 5.3d). In regions where the calcite is completely dissolved, the pH drops to that of pure water, that is, 7. Before this, equilibrium with the solid calcite phase results in a pH around 10 owing to the low buffering capacity of pure water. Figure 5.3d shows that the pH is neutralised in phase with calcium concentrations and the removal of calcite.

Pure water is not, of course, a contaminant. However, this simulation shows in a simplified way how an acidic plume would move through the soil profile, as affected by calcite buffering. With sufficient quantities of the acid solution, the soil profile's buffering capacity would be exhausted.

Saturation-dependent cation exchange with snow-plough in transient infiltration

This example investigates a cation exchange process on a typical exchange material with negative permanent charge adsorption sites during transient infiltration. The

Figure 5.3: Kinetic calcite dissolution during transient unsaturated infiltration: (a) moisture content; (b) calcium concentrations in solution; (c) solid-phase calcite; (d) pH.

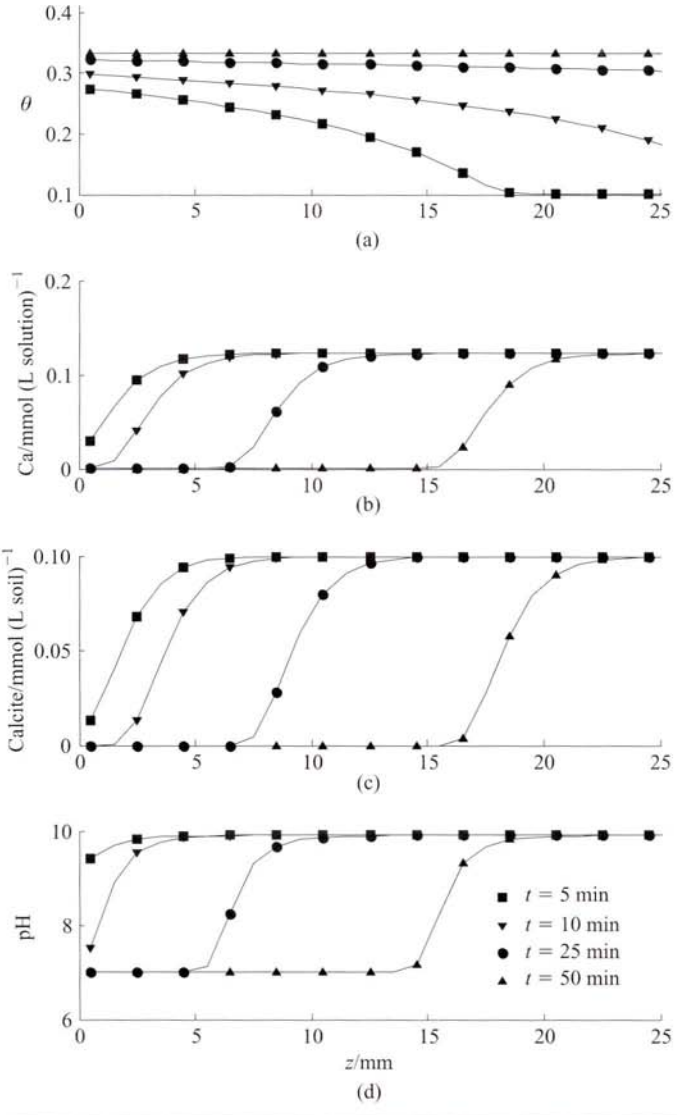

process of cation exchange has been found relevant in many clayey soils where the solid surfaces exhibit a large amount of permanent charge due to isomorphic substitution or edge site charge imbalance (e.g., Stumm and Morgan, 1996; Appelo and Postma, 2005) in the crystal structure. The process of subsequent exchange of different cations thus shares a common basis with ion chromatography as carried out in

laboratory analyses. It has been developed into an important geochemical analysis technique in natural aquifers by Appelo (1994a, 1994b).

To date, several ion exchange experiments have been conducted in unsaturated transient flow conditions (Heng *et al.*, 1999a; Allred *et al.*, 2007), but numerical simulations of this process display large uncertainties (Mansell *et al.*, 1993; Heng *et al.*, 1999b; Xie *et al.*, 2006). Compared with fully saturated flow, the case of transient unsaturated infiltration carries additional complications of:

- non-uniform water content, leading to strong differences in the local ion availability and transport velocity; and
- the accessibility of cation exchange sites, as it varies with water saturation.

The second point has not been accounted for explicitly in any previous simulations of cation exchange in transient unsaturated flow conditions. In the present model, the number of accessible adsorption sites is dynamically adjusted according to the water content such that, at residual water content, the number of exchange sites is zero, and at saturated water content it reaches the total cation exchange capacity.

In this example, sodium ions from the residual soil solution in an initially dry soil are adsorbed onto an immobile exchanger. The infiltration of a calcium chloride solution produces a distinct moisture front, in which calcium ions replace the adsorbed sodium. This displacement process, which has been referred to as *snow-plough* in the literature, leads to a concentration peak of mobile sodium in solution ahead of the infiltrating calcium. The process has been investigated numerically in saturated steady-state flow conditions (e.g., Barry *et al.*, 1983; Bajracharya and Barry, 1995).

The hydraulic properties of the soil in this simulation are those of a sandy clay loam (Šimůnek *et al.*, 2005) with $\theta_{sat} = 0.39$, $\theta_{res} = 0.1$, $\alpha_g = 0.0059\ \text{cm}^{-1}$, $n_g = 1.48$, and $K_{sat} = 0.0218\ \text{cm min}^{-1}$.

The initial and boundary conditions are

$$\begin{aligned} &t = 0,\ z \geqslant 0,\ \theta = 0.12 && C = c_{ini} \\ &t \geqslant 0,\ z = 0,\ q = 10^{-5}\ \text{m min}^{-1} && C = c_0 \\ c_{ini}\text{: } &[Ca^{+2}] = 0,\ [Cl^{-1}] = 0,\ [Na^{+}] = 10^{-5},\ [Cl^{-}] = 10^{-5} \\ c_0\text{: } &[Ca^{+2}] = 5 \times 10^{-4},\ [Cl^{-}] = 10^{-3},\ [Na^{+}] = 0,\ [Cl^{-}] = 0 \end{aligned} \tag{5.33}$$

Figure 5.4 illustrates the simulation results at times 50, 150 and 250 h after beginning of infiltration. Figure 5.4a shows the proceeding moisture front, which reaches the zero-gradient lower boundary after about 150 h.

The solution concentration of exchanging cations is shown in Figure 5.4b. Since anions are unaffected by the exchange process, they are not displayed. Inflowing calcium concentrations are strongly retarded compared with the moisture front, because free calcium adsorbs onto permanent charge sites owing to the strong affinity of the exchanger for divalent ions. In return, sodium is released into the soil solution. Owing to the strong preference of common cation exchangers towards calcium, sodium concentrations in solution do not strongly influence the exchange process. The difference in affinity is also responsible for the strong gradient in the concentration

Figure 5.4: Cation exchange process during transient unsaturated infiltration: (a) moisture content; (b) solution ions; (c) exchanger composition.

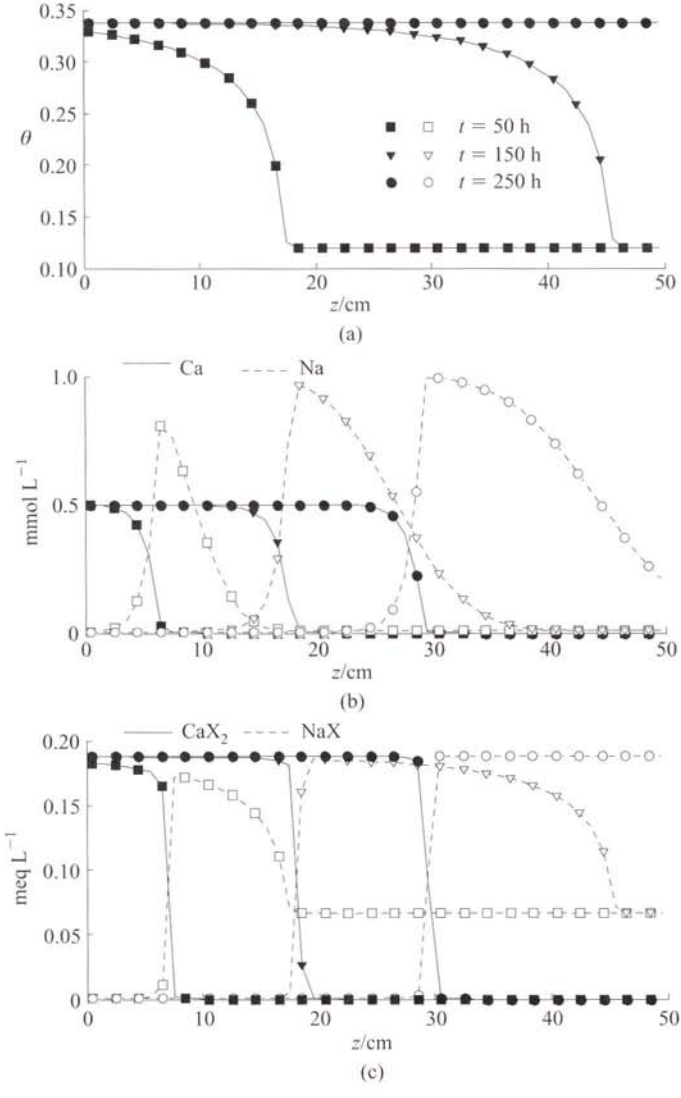

front, whereas the total number of permanent charge sites (CEC) dictates the retardation of calcium compared with the moisture front. If the number of exchange sites is large compared with equilibrated ion concentration in the initial solution and affinities of the exchanging ion are high, desorbed ion concentrations exceed initial concentrations by far. This produces the distinct concentration peak of sodium that is observed in the figure.

Figure 5.4c shows the composition of the water accessible exchanger in equivalents. In contrast to variable charge sites, negative permanent charge sites have to be occupied by a charge-balancing ion. If only sodium is present, as is the case in the initial solution, the entire exchanger is filled with sodium ions. The sharp transition between the sodium- and calcium-filled exchangers is due to the aforementioned larger affinity of the exchanger for calcium. The sum of equivalents of both exchange species yields the accessible exchange capacity, which is taken to be linearly dependent on the moisture content in this simulation.

Surface adsorption on variable-charge sites including immobile diffuse double layer

Variable-charge solids adsorb ions from the solution without releasing other ions in equivalent proportions, as is the case for the ion exchange processes described above. They are important in regulating the mobility and therefore the environmental impact of both positively charged metals and oxyanions such as $HAsO_4^{2-}$ and SO_4^{2-} (Appelo and Postma, 2005). The scheme's capability of simulating unsaturated reactive solute transport together with pH- and ionic-strength-dependent surface adsorption is demonstrated with a simple case involving reactive surfaces and equilibrium dissolution of calcite. The electrostatic diffuse double layer model (Dzombak and Morel, 1990) as implemented in PHREEQC iteratively computes the composition of adsorption sites, the resulting surface charge and ion composition in the adjacent diffuse layer according to the Donnan model (Tipping and Hurley, 1992; Kinniburgh *et al.*, 1999). The solution in the diffuse layer is excluded from flow and solute transport calculations and therefore considered immobile.

The initial and boundary conditions of the simulation are specified, together with the hydraulic and geochemical properties of the column, in Table 5.2.

The included geochemical reactions are solution speciation mineral dissolution of calcite and surface adsorption onto two surface types with different binding characteristics. Surface species and binding characteristics are those of hydro-ferric oxides as derived from a compilation of experimental studies by Dzombak and Morel and included in the MINTEQ database (version 2; http://www.lwr.kth.se/English/OurSoftware/vminteq/; distributed with PHREEQC).

Figure 5.5a shows the infiltration front and rapidly changing pH due to infiltration of the strongly alkaline solution. The slight buffering at pH around 10 results from a combination of calcite dissolution and calcium complexation. Free calcium ions provided by the dissolution process replace hydrogen ions from the surface functional groups. The release of hydrogen from the surface buffers the pH until the buffering capacity of surface sites is exhausted.

Figure 5.5b shows the solution concentrations for sodium, carbonate and calcium. Comparing the front positions of sodium and water, it is apparent that the solute is retarded even though it is not directly involved in any surface reactions. Retardation of sodium is due to the complete replacement of the initial water by the inflowing solution (Smiles and McOrist, 2001). In the numerical model, perfect mixing between the inflowing and the initial solution in a cell is assumed. The increasing pulse of free carbonate concentrations results from the progressive dissolution of calcite at the pH

Table 5.2: Model specification for variable charge surface adsorption in transient, unsaturated flow conditions. Units of ion concentrations are mol (L solution)$^{-1}$; units of equilibrium phases and surface sorption sites are mol (L soil)$^{-1}$.

Discretisation	
Number of cells	50
Cell size, Δz	1 mm
Transport time step, Δt	0.01 day
Hydraulic properties (van Genuchten parameters for loamy sand)	
α_g	0.0124 mm^{-1}
n_g	2.28
K_{sat}	0.040 532 424 mm day^{-1}
θ_{sat}	0.41
θ_{res}	0.0124 mm^{-1}
Geochemical properties (surface assembly and solid phase in equilibrium with initial solution	
Equilibrium phases	
Calcite	1.152×10^{-2}
Surface properties	
Weak adsorption sites (Hfow)	0.02
Strong adsorption sites (Hfos)	5×10^{-4}
Specific surface area	600 m^2 g^{-1}
Total mass of surface in each cell	0.03 g
Thickness of diffuse layer	10^{-8} m
Initial solution	
pH	7.126
Ca^{2+}	2.080×10^{-3}
Na^+	7.877×10^{-7}
CO_3^{2-}	4.779×10^{-3}
Water content	0.1 kg
Conditions at the inflowing boundary	
pH	13.2
Na^+	2.421×10^{-1}
Water content	0.4 kg

front. Calcium concentrations are controlled by dissolution of calcite and surface adsorption. The large amounts of surface sites adsorb most of the free calcium at high pH and therefore shift the ion activity product for calcite towards carbonate. Amounts of sodium, calcium and carbonate in the diffuse double layer (not shown) are negligible, while the concentration of carbonate is an order of magnitude smaller, owing to co-ion exclusion.

Figure 5.5c shows the total amount of solid-phase calcite. The large extent of calcite dissolution at the pH front is due to the complexation of free calcium. The

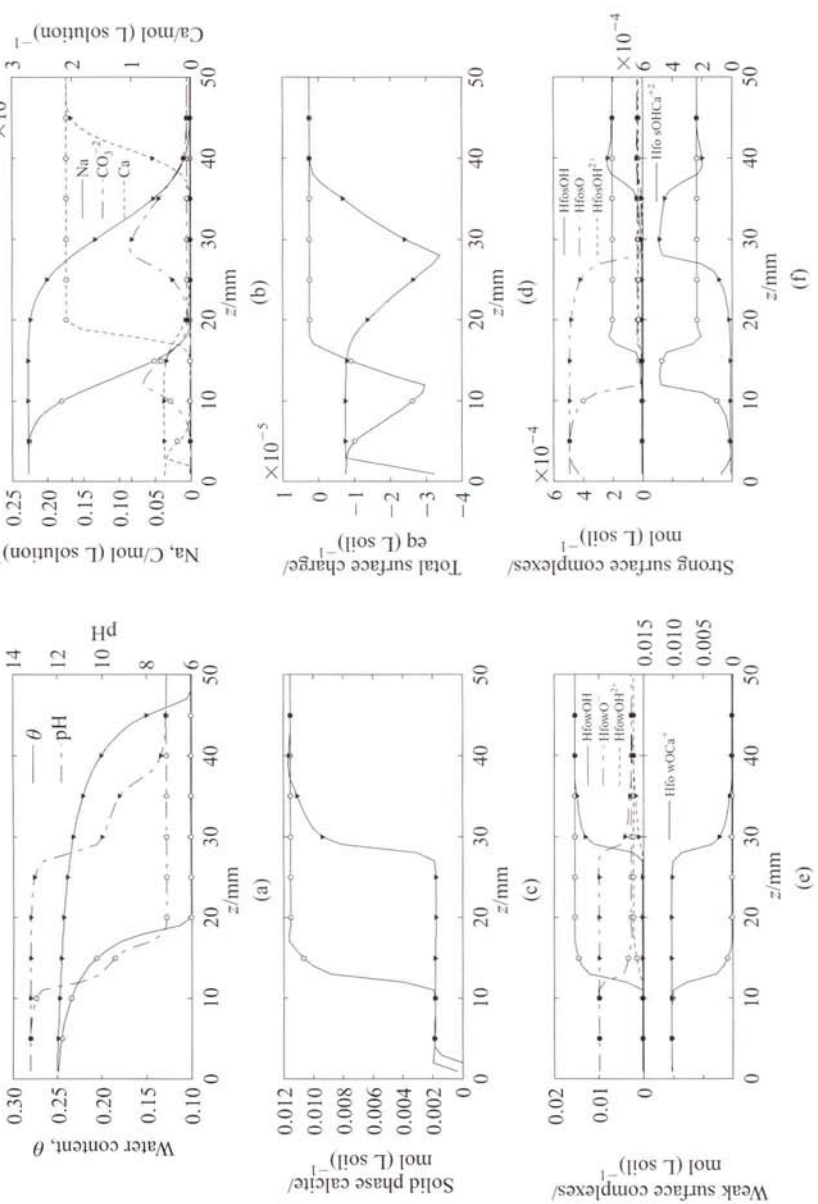

Figure 5.5: Transient infiltration of hyperalkaline solution with surface adsorption and equilibrium phase reactions after 40 days (circles) and 200 days (triangles): (a) water content and pH; (b) solution ions; (c) solid-phase calcite; (d) total surface charge; (e) weak surface complexes; (f) strong surface complexes.

dramatic pH change reduces the ion activity product of carbonate and calcium, owing to the surface complexation of calcium ions, and thus increases calcite dissolution. This explains the progress of the primary dissolution front with the velocity of solute transport. Without the adsorption mechanism only about 1.66×10^{-4} moles of calcite are soluble in 0.4 kg water at a pH of 13.2. These small amounts of calcite continuously dissolve close to the inflow boundary owing to the intrusion of chemically undersaturated solution. Because of the equilibrium assumption, dissolution takes place only in the first cell that contains calcite. This explains the slow progress of the secondary dissolution front.

From Figure 5.5d it can be seen that the high pH of the infiltrating solution produces a change in surface charge from slightly positive values at the initial pH towards predominantly deprotonated, negative surface sites. In the presence of calcium ions, the negative charge sites are filled, which ameliorates the surface charge to mildly negative values. However, in the regions with high pH and no adsorbing ion, the surface charge decreases dramatically.

Figure 5.5e shows the composition of the weak surface sites with progressively decreasing amounts of protonated and neutral surface species. Behind the solute front, roughly half of the weak surface sites form calcium complexes and therefore acquire a net positive charge. The other half consists of negative, deprotonated sites.

The strong surface sites in Figure 5.5f show a sequence of adsorption. Calcium ions are coordinated by neutral surface sites immediately behind the solute front, increasing the overall surface charge. After the pulse of carbonate in the solution reaches its peak, calcium and hydrogen ions desorb from the surface, leaving deprotonated sites with a negative charge.

The geochemical conditions in the column change as soon as the solid calcite is dissolved and flushed from the column. Calcium desorption processes take place, which can only be observed near to the inflow boundary.

Even in this relatively simple system, strongly interacting processes with complex feedback reactions take place. Surface adsorption influences mineral dissolution. The solution ions released by mineral dissolution determine the composition of surface sites. Surface adsorption and mineral dissolution are controlled by the pH and at the same time act as pH controls through release or uptake of pH-affecting species. Understanding all these interacting processes, together with the development of a diffuse double layer and its influence on water and ion mobility in unsaturated flow conditions, without the help of detailed simulations is difficult if not impossible.

5.3 BIO-CLOGGING

In reactive transport modelling, biological and inorganic geochemical reactions are often assumed to induce only small changes in the physical structure of the porous medium. As a result of this assumption, the feedback on the water flow field is assumed negligible. In a number of cases, however, this assumption may not be adequate, and a "two-way" coupling must be incorporated into models of water flow and biochemical reactions.

Fundamentally, biogeochemical processes produce changes in the structure of the pore space that result in modifications of both the available (mobile) porosity and the tortuosity of the flow paths. In turn, these changes result in modification of the hydraulic conductivity and dispersivity of the porous medium (Taylor and Jaffé, 1990; Baveye *et al.*, 1998). Further to this, for unsaturated flow, changes in the pore-throat diameter distribution also lead to modification of the characteristic retention function. When these modifications lead to the reduction of porosity and hydraulic conductivity, the process is commonly referred to as *pore clogging*. Several chemical and physical processes, possibly mediated by the biomass, can produce temporary or permanent modifications of the porous structure. Among these, the most important can be summarised as

- growth of biomass,
- formation of gas bubbles,
- precipitation of mineral phases, and
- filtration (i.e., deposition of fine particles and colloids suspended in the pore fluid).

In many cases all these phenomena occur simultaneously, and lead synergistically to larger modification of the hydrodynamic properties of the soil or porous medium than individual processes (Baveye *et al.*, 1998; Cooke *et al.*, 2001; Breadford *et al.*, 2003; Amos and Mayer, 2006).

Pore clogging has many adverse environmental effects, and can result in poor engineering results. For example, wastewater treatment technologies that make use of sand filters (e.g., constructed wetlands) are potentially affected by clogging as a result of biomass growth due to the availability of carbon sources and nutrients in urban and agricultural discharged waters. The reduction of hydraulic conductivity in turn adversely affects treatment efficiency and energy consumption (Reddi *et al.*, 2000; Rowe *et al.*, 2000; Islam *et al.*, 2001; VanGulck and Rowe, 2004). Technologies for *in situ* treatment of contaminated groundwater also often lead to a modification of the hydrodynamic properties of the porous matrix. For example, during remediation of contaminated soil and groundwater using air sparging, pore clogging leads to the formation of preferential flowpaths, and as a result significant regions of the soil can remain untreated (Baveye *et al.*, 1998; Kalin, 2004; Seki *et al.*, 2006; Brovelli *et al.*, 2009). Clearly, in many engineering applications, particularly those aimed at maximising the efficiency of the remediation, it will be necessary to consider pore clogging carefully, and to incorporate these processes into relevant models.

In this section we shall describe pore-clogging processes and present a general modelling approach to simulate clogging for the case where the changes of the hydrodynamic properties of the soil result from an increase or decay of biomass (Brovelli *et al.*, 2009). The same modelling approach may be also applied to simulate clogging due to other mechanisms, such as the formation of gas bubbles or precipitation of a solid phase. This can be accomplished by replacing the equations describing the changes in biomass volume with the relevant geochemical/physical model of interest. For the sake of clarity, only saturated flow conditions will be considered. That is, the model's domain of application is groundwater aquifers. Because the method-

ology we present is process based, it can be used to simulate remediation strategies and, for example, contribute to the design and optimisation of such schemes.

5.3.1 Model formulation for pore clogging in saturated porous medium

On a macroscopic scale (e.g., Clement *et al.*, 1997; Kildsgaard and Engesgaard, 2001; Brovelli *et al.*, 2009), using a simple volume balance, the fraction of pore space accessible for water flow and solutes at any time – that is, the mobile porosity ϕ_{mob} – is computed by

$$\phi_{\text{mob}}(X_s) = \phi_0 - \phi_{\text{imm}}(X_s) \tag{5.34}$$

where ϕ_0 is the initial porosity of the clean porous medium, and $\phi_{\text{imm}}(X_s)$ is the fraction of pore space that has been filled or eroded as a consequence of the biological or geochemical reactions. The variation of porosity is a function of the mass of immobile phase removed or deposited:

$$\phi_{\text{imm}}(X_s) = \sum_{i=1}^{n} \frac{X_s^i \rho_b}{\rho_s^i} \tag{5.35}$$

where X_s^i is the dry weight mass of the ith component of the immobile phase per unit mass of aquifer solids; ρ_b (M L^{-3}) is the initial bulk density of the porous medium; and ρ_s^i (M L^{-3}) is the density of the ith component of the immobile phase. Equations 5.34 and 5.35 provide a general framework to model porosity changes due to an arbitrary number of aquifer components. In order to model bio-clogging, X_s must be set to the dry weight of biomass growing in the porous medium.

Modelling biomass

In porous media, bacteria are present both as separate cells dispersed in the pore fluid and as immobile aggregates attached to the matrix of the porous medium. Only immobile biomass contributes to changes in the pore volume and thus to clogging. However, interchange between mobile and immobile concentrations is possible by attachment and detachment processes, and these have to be considered.

Classically, biomass growth is assumed to follow Michaelis–Menten-type behaviour (e.g., Barry *et al.*, 2002), while cell decay is considered a first-order kinetic process. These assumptions have proved suitable for reproducing biomass dynamics in a large number of situations, including those where clogging plays a significant role. For example, in the case where the substrate (electron donor and C source) and electron acceptor availability are limiting factors, then the overall biomass growth rate can be expressed as

$$\mu = \mu_{\max}\left(\frac{C_{ea}}{K_{ea} + C_{ea}}\right)\left(\frac{C_s}{K_s + C_s}\right) - k_d \tag{5.36}$$

where μ (T^{-1}) is the specific growth rate; $\mu_{\max}$ (T^{-1}) is the maximum growth rate; C (M L^{-3}) is the concentration; K (M L^{-3}) is the half-saturation constant; the subscripts

ea and s stand for electron acceptor and substrate, respectively; and k_d (T^{-1}) is the first-order biological decay constant.

When modelling bio-clogging, an additional inhibition term needs also to be considered to account for the limited supply of nutrients as the biomass grows and fills the pore space (Kindred and Celia, 1989; Prommer and Barry, 2005). A mathematical expression was suggested by Zysset *et al.* (1994):

$$I_{bio} = \frac{X_s^{max} - X_s}{X_s^{max}} \tag{5.37}$$

where X_s^{max} is the biomass-holding capacity of the porous medium, that is, the largest possible amount of biomass that can grow in the pores. An upper bound for this parameter is given by the available pore space. In practice, however, nutrient supply becomes the limiting factor for biomass growth before all the pore space is filled with biomass, and the holding capacity is thus smaller than its theoretical upper limit.

Incorporating the biomass inhibition factor in Equation 5.37, Equation 5.36 can be generalised to

$$\mu = \mu_{max} I_{bio} \sum_{i=1}^{N} \frac{C_i}{K_i + C_i} - k_d \tag{5.38}$$

with N being the number of limiting components. A detailed review of other possible mathematical expressions for the growth and decay process is available (Barry *et al.*, 2002).

Attachment and detachment processes are comparatively less well understood, and only a small number of theoretical studies have been carried out to elucidate the effect of various chemical and physical characteristics on attachment and detachment processes modifying the porous medium and the pore-water transport. Most of the suggested theoretical equations describing these processes contain inconsistencies that limit model applicability and robustness (Tufenkji, 2007). The more frequently used equations are still based on colloid filtration theory, which arguably has limited applicability to bacteria motility (Rittmann, 1982; Harvey and Garabedian, 1991; Reddi *et al.*, 2000; Tufenkji, 2007). Despite these weaknesses, these equations have been extensively used (e.g., Clement *et al.*, 1996; Kildsgaard and Engesgaard, 2001; Thullner *et al.*, 2004) to model the interchange of biomass between the immobile and mobile phases. The attachment coefficient, k_{att} (T^{-1}), can be computed as (Harvey and Garabedian, 1991; Scheibe *et al.*, 2007)

$$k_{att} = \frac{3(1-\phi)v_p\eta}{2d_g} \tag{5.39}$$

where v_p (LT^{-1}) is the pore-water velocity; d_g (L) is a characteristic grain diameter; and η is the collector efficiency, a parameter representing the frequency of collisions between mobile bacteria and grain surfaces. Closed-form relationships have been proposed to compute the collector efficiency (Tien *et al.*, 1979; Scheibe *et al.*, 2007), but such equations contain parameters that cannot be easily computed directly, and

consequently the collector efficiency is normally estimated by fitting experimental data.

While all the previous modelling studies agree on the importance of the attachment rate, the sensitivity and importance of shear detachment have been widely debated, and no unique approach can be identified to estimate its value. According to Thullner *et al.* (2004), shear detachment can be safely neglected, at least when the flow field is two-dimensional. Kildsgaard and Engesgaard (2001) also considered a two-dimensional flow field and found good agreement between experimental and simulation results by dropping the dependence on flow velocity. This result can be explained by considering that, as the porous medium becomes locally blocked, water flow can circumvent the low-conductivity area. The resulting increase in flow velocity is consequently only limited, and so is the variation of shear stress. A general, semi-empirical equation to compute the detachment rate is (Rittmann, 1982)

$$k_{\mathrm{det}} = c_{\mathrm{d}} \left[\frac{\gamma v_{\mathrm{p}} (1-\phi)^3}{d_{\mathrm{p}}^2 \phi^3 M} \right]^{0.58} \tag{5.40}$$

where k_{det} (T^{-1}) is the detachment rate, γ ($\mathrm{M\,L^{-1}\,T^{-1}}$) is the dynamic viscosity of water, M (L^{-1}) is the specific surface area of the porous medium, and c_{d} is an empirical dimensionless parameter. By calibrating Equation 5.40 with some experimental datasets, Rittmann (1982) proposed a value of $c_{\mathrm{d}} = 2.29 \times 10^{-6}$. At present, shear detachment can be estimated only by calibration with experimental measurements.

Combining these different processes, the coupled ordinary differential equations describing mobile and immobile biomass variation in time may be written as

$$\frac{\partial X_{\mathrm{imm}}}{\partial t} = \mu_{\mathrm{imm}} X_{\mathrm{imm}} - k_{\mathrm{det}} X_{\mathrm{imm}} + k_{\mathrm{att}} X_{\mathrm{mob}} \tag{5.41}$$

$$\frac{\partial X_{\mathrm{mob}}}{\partial t} = \mu_{\mathrm{mob}} X_{\mathrm{mob}} + k_{\mathrm{det}} X_{\mathrm{imm}} - k_{\mathrm{att}} X_{\mathrm{mob}} \tag{5.42}$$

where the subscripts imm and mob refer to the solid, immobile biomass and the mobile, free-floating biomass in the aqueous phase, respectively.

Constitutive models linking saturated permeability to porosity change

The relationship linking saturated permeability to porosity changes is non-trivial and difficult to define. Saturated permeability depends on a large number of microstructural and geometrical properties of the porous structure, such as pore size distribution, pore shapes, connectivity and tortuosity. None of these properties can be deduced directly from the changes in the porosity, and depend primarily on the biomass configuration and distribution at the pore scale. A number of constitutive relationships have been proposed, such as the well-known Kozeny–Carman relationship, but none has found general applicability (e.g., Zheng and Bennett, 2002). A subset of these relationships has been developed to account for the properties of the biomass aggregates (e.g., Vandevivere *et al.*, 1995; Baveye *et al.*, 1998). Among the best

known are the colonies (Taylor and Jaffé, 1991) and biofilm models (Clement *et al.*, 1996; Thullner *et al.*, 2002). Using a simplified description of both the porous medium and the biomass, these relationships were found suitable to reproduce the clogging patterns observed in several experiments.

The simplest relationship takes the form (Ives and Pienvichitr, 1965; Okubo and Matsumoto, 1979; Knapp *et al.*, 1988; Clement *et al.*, 1996)

$$K_{\mathrm{rel}}(\phi_{\mathrm{rel}}) = \phi_{\mathrm{rel}}^{p} \tag{5.43}$$

where K_{rel} and ϕ_{rel} are the (dimensionless) relative hydraulic conductivity and relative porosity at a given time. The relative porosity is defined as the ratio of current porosity and the corresponding value for the clean porous medium – that is, in the absence of clogging. The value of p depends on the characteristics of the porous medium. Clement *et al.* (1996) derived Equation 5.43 analytically and showed that the exponent is a function of the pore-size distribution. No assumptions were made regarding the properties of biomass in the porous medium. For porous media consisting of cylindrical pores with effective length proportional to the pore radii, Clement *et al.* (1996) suggested that the exponent should be set to $p = \frac{19}{6}$ With this condition, the model of Clement *et al.* (1996) is completely equivalent to that of Taylor and Jaffé (1991).

Using a pore-network approach on heterogeneous digital porous media, Thullner *et al.* (2002) proposed two analytical expressions for different configurations of the biomass. The underlying assumption of both models is that bacteria grow in the smallest pores first. One such constitutive equation is the aforementioned colonies model. It assumes that the immobile biomass grows in isolated patches, and is described by the expression

$$K_{\mathrm{rel}}(n_{\mathrm{rel}}) = a_0 \left(\frac{\phi_{\mathrm{rel}} - n_0}{1 - n_0}\right)^3 + (1 - a_0)\left(\frac{\phi_{\mathrm{rel}} - n_0}{1 - n_0}\right)^2 \tag{5.44}$$

where a_0 and n_0 are dimensionless adjustable parameters, with $1 - n_0$ being interpreted as the relative volume of biomass needed to obtain the maximum reduction of hydraulic conductivity: in other words, the hydraulic conductivity becomes negligible as the relative porosity ϕ_{rel} approaches n_0. Theoretical considerations have proved that Equation 5.44 is valid only when the parameter a_0 assumes a value between -2 and -0.5 (Thullner *et al.*, 2002). Fitting of Equation 5.44 to experimental data shows reasonably good agreement (Thullner *et al.*, 2002, 2004). The parameter n_0 was found in most cases to lie in the range 0.4–0.9, while a_0 was found to lie between -1 and -1.9.

In contrast to the colonies approach, the biofilm model assumes a single, connected layer of biomass covering the wall of each pore. As a consequence of biofilm development, the pore radius is reduced, and therefore also water flow and solute transport are subsequently modified. This relationship assumes the form

$$K_{\mathrm{rel}}(\phi_{\mathrm{rel}}) = \left[\left(\frac{\phi_{\mathrm{rel}} - n_0}{1 - n_0}\right)^b + K_{\min}\right]\left(\frac{1}{1 + K_{\min}}\right) \tag{5.45}$$

where b is a dimensionless fitting parameter, and $K_{\min}$ is the lower limit for the relative hydraulic conductivity – that is, the value of relative hydraulic conductivity as ϕ_{rel} approaches n_0. Application of the biofilm model to experimental data resulted in a good fit (Thullner *et al.*, 2002, 2004), with the values for n_0 in the range 0.2–0.4 and 6×10^{-3} to 10^{-2} for $K_{\min}$.

Figure 5.6 compares the three constitutive relationships. In Figure 5.6a, the colonies model of Thullner *et al.* (2002) is plotted together with the Clement model, that is, Equation 5.43 with exponent $\frac{19}{6}$. For the same porosity decrease, the corresponding permeability reduction differs significantly for any value assumed by the parameters. In contrast, the biofilm model (Equation 5.45) exhibits an exponential behaviour and, depending on the value of the exponent, it may be very similar to the model of Clement, as depicted in Figure 5.6b. A great advantage of the biofilm model of Thullner *et al.* (2002) is that, while maintaining the power-law behaviour that has been often observed in the experiments (e.g., Sahimi, 1995), it has some adjustable parameters that increase its flexibility.

The physical characteristics of these bio-clogging models are presented in the following examples.

5.3.2 One-dimensional example: laboratory column experiment

The first example studies a case with one-dimensional bio-clogging. It is designed to illustrate the temporal and spatial evolution of hydraulic properties under one-dimensional flow conditions, as may be encountered in small-scale laboratory experi-

Figure 5.6: Comparison of the constitutive models and parameter sensitivity. (a) Comparison of the colonies model of Thullner *et al.* (2002) with the power law (Equation 5.43). (b) Comparison of the power law with the biofilm model. The exponent is set to $\frac{19}{6}$, as suggested by Clement *et al.* (1996).

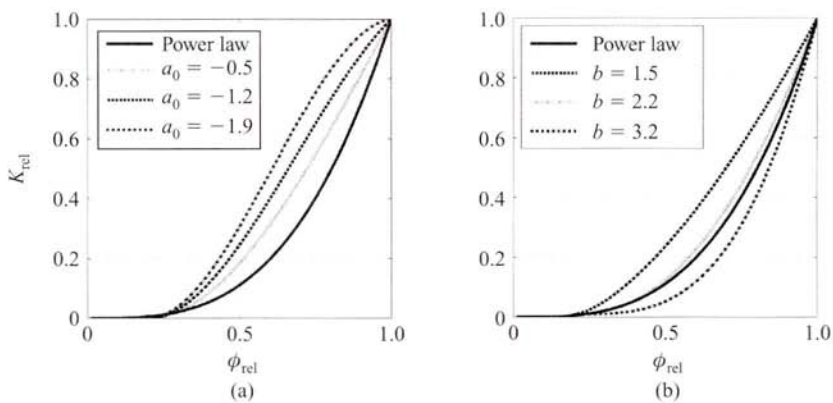

ments. Soil column experiments are often used to evaluate the behaviour of natural compounds or contaminants. However, it has been observed in numerous situations that clogging easily occurs. Unless considered explicitly, bio-clogging may seriously limit the interpretability of the results of such experiments.

A soil column experiment is simulated for the case of a constant water flow rate at the inlet boundary, and fixed hydraulic head at the outlet. Biomass growth is controlled only by the availability of the carbon source and electron acceptor. The electron donor and nutrients are assumed not to be limiting. The porous medium is initially seeded with a constant small amount of biomass, as is typical for laboratory experiments (e.g., Taylor and Jaffé, 1991; Biefeldt *et al.*, 2002). Figure 5.7 presents the porosity and hydraulic conductivity profiles 50 and 100 days after the beginning of the experiment. In both cases, only a small fraction of the total column length has significantly different hydraulic properties (0.05 m and 0.1 m, respectively). Figure 5.8 reports the bulk hydraulic conductivity as a function of time, computed from the head difference between the inlet and outlet. After an initial phase (of about 15 days) where the conductivity remains constant, a sharp drop of the conductivity is observed, of several orders of magnitude. Such behaviour is often observed in the laboratory (e.g., Taylor and Jaffé, 1991; Biefeldt *et al.*, 2002), and is due to two factors: the relationship between porosity and hydraulic conductivity is non-linear, and the biomass has exponential growth. After this sharp decrease, the rate of further hydraulic conductivity change is strongly reduced. On comparing Figures 5.7 and 5.8, it is clear that the bulk hydraulic conductivity is controlled by the properties near the inlet.

Figure 5.7: (a) Porosity and (b) hydraulic conductivity profiles for the one-dimensional simulated column experiment. The solid lines show simulated results at 50 days, and the dots are relevant to 100 days.

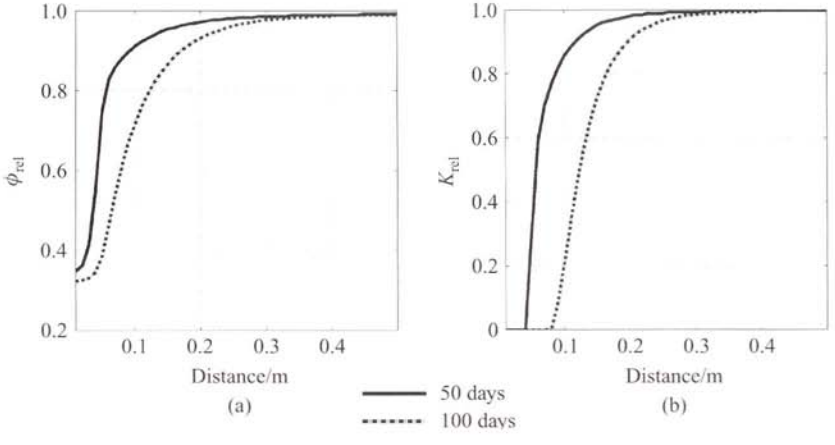

Figure 5.8: Evolution of the bulk hydraulic conductivity for the simulated column. The bulk conductivity depends strongly on the conductivity of the clogged zone near the inlet.

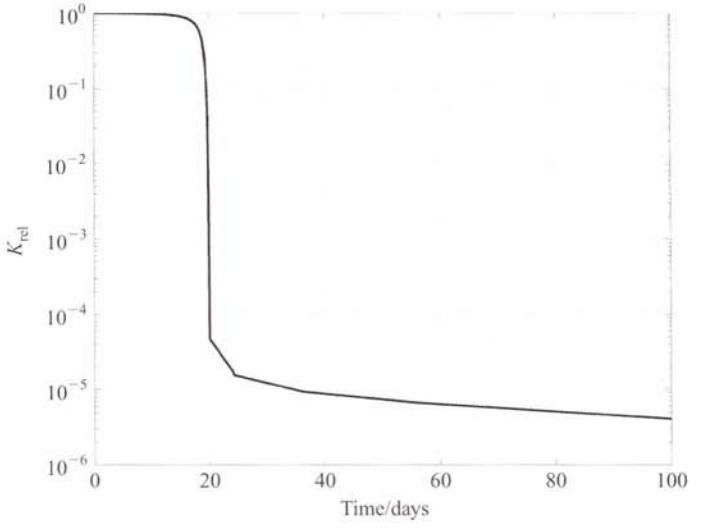

5.3.3 Two-dimensional example: clogging of a bioreactive barrier

The second example illustrates the effect of clogging on the remediation of contaminated groundwater with a reactive barrier. Figure 5.9 is a sketch of the problem to be solved numerically. To remove an organic contamination from the groundwater, a passive engineered bioreactive barrier is built downstream from the contamination source. Bioreactive barriers are relatively novel *in situ* remediation technologies that make use of natural processes to clean the groundwater, and have found increasing success in the last few years (e.g., Kalin, 2004). In fact, the word "barrier" is a misnomer, since its purpose is to draw contaminated water towards it. The barrier consists of a support material with high hydraulic conductivity, inoculated with selected strains of bacteria. Deterioration of the performance of the barriers with time due to pore-clogging induced by biomass growth and accumulation of fines and inorganic particles has been observed in some cases (Kalin, 2004; Seki *et al.*, 2006).

In this example we simulate the behaviour of a biological reactive barrier, as shown in Figure 5.9. We consider a simplified biogeochemical model, with the contaminant acting as carbon source for biomass growth. Two situations are studied. In the first case, bio-clogging is incorporated in the simulation, whereas in the second the same biological model is used, but it is assumed that porosity and hydraulic conductivity variations are negligible. Figure 5.10 shows the total contaminant recovery downstream of the reactive barrier for the two situations. The recovery rate is computed as the ratio between the total mass of contaminant along two transects, one

Figure 5.9: Schematic representation of the numerical model used in the second bio-clogging example. The distance between the contaminant source and the permeable reactive barrier is 50 m. Fixed-head boundary conditions are used both for the inlet and the outlet.

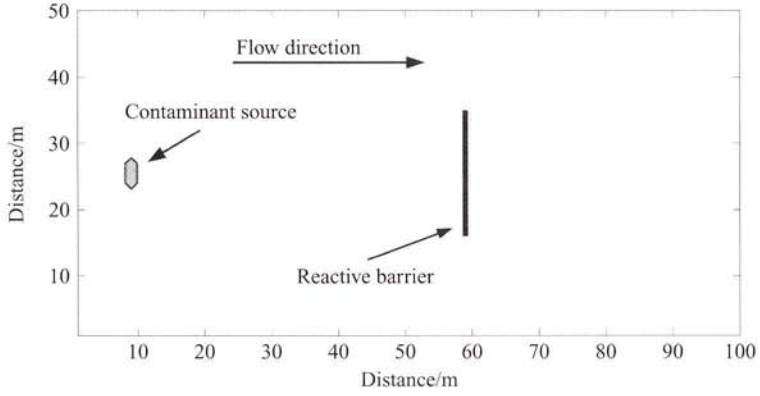

Figure 5.10: Fraction of the recovered contaminant as a function of time for the two cases. The recovery rate is computed as the ratio between the injected contaminant and the integral concentration along a transect near the model outlet. A high recovery means poor behaviour of the reactive barrier.

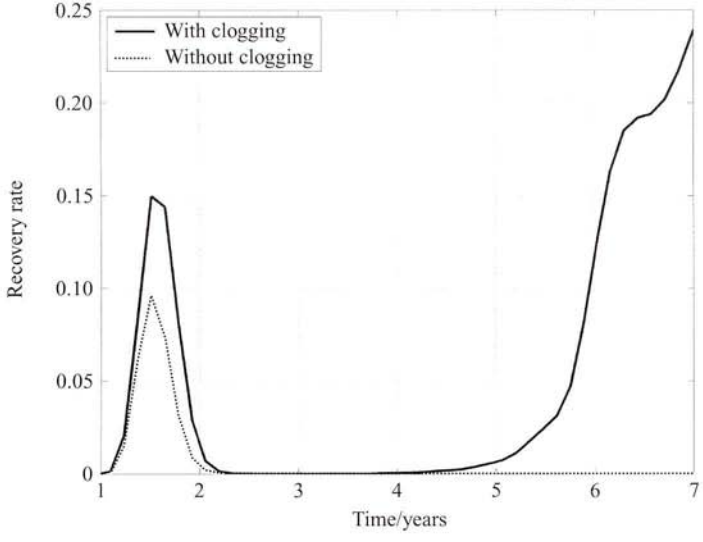

placed between the contaminant source and the barrier, the second downstream of the barrier. A high contaminant recovery indicates a poor efficiency of the treatment technology. For both cases, after about 1.5 yrs of barrier operation, a recovery peak is observed, with the maximum for the case with clogging larger than the situation when clogging is not considered. The peak shows that the contaminant reaches the barrier, and the biomass grows while consuming it. After about 1 yr, the concentration of biomass is large enough to completely degrade the contaminant, and the recovery rate drops to zero in both cases. After 4 yrs, whereas the contaminant remains completely degraded in the case without clogging, the recovery rate starts increasing in the simulation where clogging is included, and a few years later the efficiency of the barrier drops dramatically by about 25%. The reason for this behaviour can be deduced from Figure 5.11, where maps depicting the contaminant distribution are

Figure 5.11: Contaminant distribution for the case with bioclogging considered: (a) time 1 yr; (b) time 4 yrs; (c) time 8 yrs. As the hydraulic conductivity of the reactive barrier decreases, the contaminant starts flowing around the barrier instead of through the reactive zone. In consequence, the removal efficiency drops.

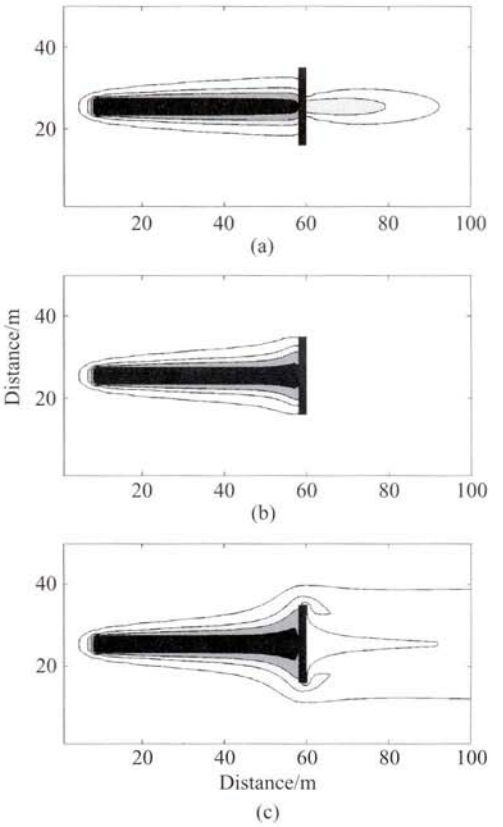

reported. Initially, when the concentration of biomass is low, the hydraulic properties of the barrier in the two cases are similar, and so is the water flow field. The contaminant flows through the central part of the barrier and is completely degraded (Figure 5.11a). After some time, in the simulation with clogging the volume of biomass increases. The result is that the hydraulic conductivity of the barrier decreases, and the contaminant plume spreads laterally. Initially (Figure 5.11b), the barrier is large enough to overcome lateral flow, and the remediation efficiency remains high. As the clogging increases further, however, the contaminant starts flowing around the barrier, and the removal efficiency drops. Although this synthetic example is simplified, it clearly illustrates that in some cases clogging plays an important role, and needs to be considered in the design of enhanced remediation schemes.

5.4 CONTAMINANT DEGRADATION IN COASTAL ZONES

Pollution of coastal waters is an increasingly serious global problem, and in recent years it has become well recognised that contaminants entering coastal waters via groundwater discharge (submarine groundwater discharge, SGD) are significant contributors to this pollution (Johannes, 1980; Simmons, 1992; Church, 1996; Moore, 1996). In some areas where serious groundwater contamination has occurred, SGD has been shown to be the dominant source of coastal pollution and thus to have considerable consequences for marine ecosystems (Johannes, 1980; Lapointe and O'Connell, 1989; Valiela *et al.*, 1990; LaRoche *et al.*, 1997). For example, discharge of groundwater with elevated nitrogen levels has been shown to accelerate eutrophication in coastal waters, leading to the initiation of intense algal blooms (Lapointe and O'Connell, 1989; LaRoche *et al.*, 1997), the loss of important habitats, and changes in marine biodiversity (Valiela *et al.*, 1990, 1992).

The flow and reactive processes in coastal aquifers can strongly control the specific transport pathway and exit conditions for subsurface contaminants discharging to coastal waters. In particular, near the shore, seawater (oxygenated) recirculating across the aquifer/ocean interface can mix with discharging fresh terrestrial groundwater (anoxic), creating an active biogeochemical reaction zone. By altering the geochemical conditions along a contaminant's discharge pathway, this mixing and reaction zone, termed a *subterranean estuary* (Moore, 1999), may influence the transformation, mobility and removal of contaminants prior to their discharge to coastal waters (Slomp and van Cappellen, 2004; Charette and Sholkovitz, 2006; Spiteri *et al.*, 2006). As a result, understanding the flow and reactive processes in coastal aquifers is crucial for accurate prediction of contaminant loading to the marine environment.

Near the shore, both seawater recirculation across the aquifer/ocean interface and subsurface flows are driven primarily by terrestrial groundwater discharge, Q_f, density-driven convection, Q_d, tidal oscillations, Q_t, waves, Q_w, and wave–bedform interactions, Q_m (Figure 5.12). The range of forcing mechanisms and their complex and dynamic interactions present significant challenges to researchers attempting to

Figure 5.12: Conceptual model of a nearshore aquifer including major seawater recirculation and groundwater flow processes: (1) fresh groundwater discharge, Q_f; (2) density-driven circulation, Q_d; (3) tide-induced circulation, Q_t; (4) wave set-up driven circulation, Q_w; (5) local circulation due to wave-bedform interaction, Q_m. Shading (grey) depicts a typical salinity distribution in a nearshore aquifer subject to oceanic forcing.

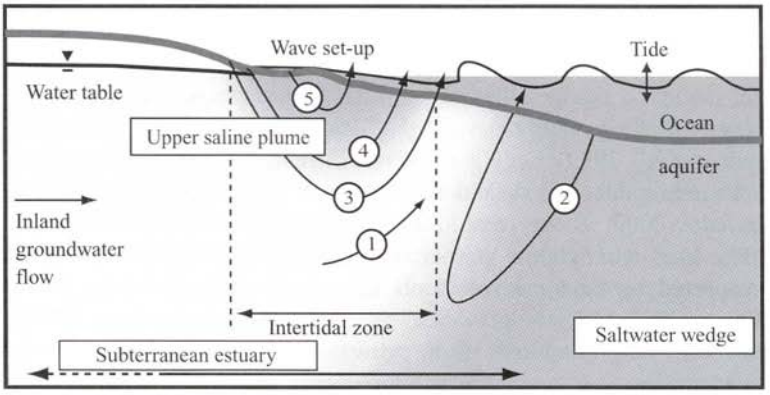

Source: Reprinted from Robinson, C., Li, L. and Barry, D.A. (2007b). Effect of tidal forcing on a subterranean estuary. *Advances in Water Resources*. 30: 851–865. With permission from Elsevier.

monitor and predict the behaviour of these systems. Accordingly there are few published field measurements of intertidal subsurface flow (Riedl and Machan, 1972; Robinson *et al.*, 2006, 2007a; Taniguchi *et al.*, 2006) and even fewer of the hydrodynamics coupled with the geochemical conditions in the aquifer. Despite the simplifications required, modelling is able to provide valuable insight into the processes in coastal aquifers and thus the potential impact of groundwater contamination on the receiving coastal ecosystem. Because a large proportion of the world's coastlines are exposed to significant tidal fluctuations, our discussion here focuses on tidally influenced coastal aquifers. The influence of waves and longer-period forcing (e.g., seasonal oscillations and groundwater mining) are therefore neglected.

5.4.1 Tide-induced groundwater flow and salt transport dynamics

Since the work of Ghyben (1899) and Herzberg (1901), researchers have attempted to model quantitatively the flow of fresh and saltwater within coastal aquifers. Historically, the primary objective was to predict the encroachment of saltwater into aquifers, which were often a valuable source of freshwater (Reilly and Goodman, 1985). In the last 20 years, however, the environmental implications of SGD have become evident, and numerous models have now been developed to predict its magnitude (Destouni and Prieto, 2003; Smith, 2004; Prieto and Destouni, 2005; Wilson, 2005), and also to

understand the mechanisms influencing the fate of chemicals in coastal aquifers (Spiteri *et al.*, 2008). The dispersion zone of the saltwater wedge, formed by density variations between seawater and fresh groundwater, has traditionally been viewed as the primary area for salt–freshwater mixing and thus for geochemical transformations in coastal aquifers (Moore, 1999). Recent measurements demonstrate, however, that seawater recirculation driven by tidal oscillations may also create an important subsurface salt–freshwater mixing zone (Robinson *et al.*, 1998, 2006; Boufadel, 2000; Vandenbohede and Lebbe, 2005).

Initial studies on tidally influenced aquifers focused largely on tide-induced water table fluctuations (e.g., Parlange *et al.*, 1984; Nielsen, 1990; Li *et al.*, 1997; Raubenheimer *et al.*, 1999). Only in more recent years have models have been used to examine the tide-induced flow and salt transport processes (Ataie-Ashtiani *et al.*, 1999; Boufadel, 2000; Zhang *et al.*, 2001; Chen and Hsu, 2004; Vandenbohede and Lebbe, 2005; Mao *et al.*, 2006a; Werner and Lockington, 2006). A series of modelling studies supported by field measurements are presented by Robinson *et al.* (2006, 2007a, 2007b, 2007c). These provide detailed understanding of the effect of tidal fluctuations on the groundwater flow, seawater recirculation and salt–freshwater mixing mechanisms in a nearshore aquifer over a range of hydrological, tidal and aquifer conditions. The numerical model used was based on the density-dependent groundwater flow code SEAWAT-2000 (Langevin *et al.*, 2003). Tidal forcing across the sloping beach boundary was simulated using a surface water zone and an aquifer zone. A schematic of the model domain, including an example of the boundary conditions and basic parameter set used, is shown in Figure 5.13. Further details of the model are provided in Robinson *et al.* (2007b).

Figure 5.13: Model geometry, boundary conditions and basic parameter set. The model domain is divided into two zones: a surface water zone and an aquifer zone. Time-varying head cells in the surface water zone are used to implement the tidal condition (amplitude = 1 m).

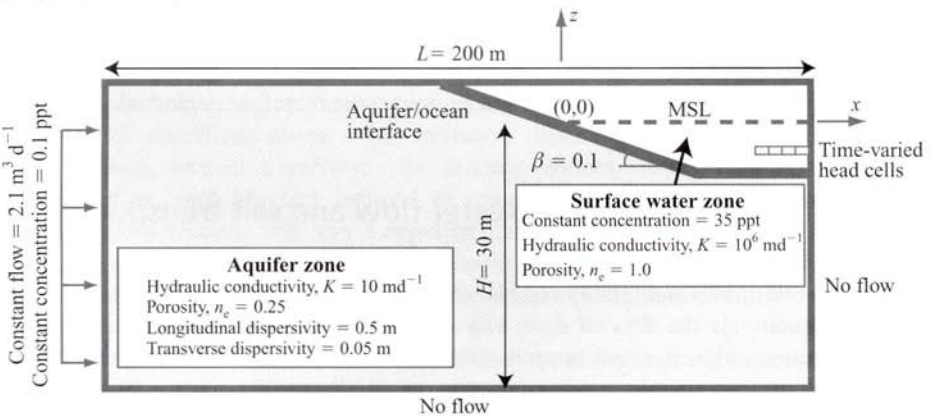

Source: Reprinted from Robinson, C., Li, L. and Barry, D.A. (2007b). Effect of tidal forcing on a subterranean estuary. *Advances in Water Resources*. 30: 851–865. With permission from Elsevier.

Tidal fluctuations induce oscillatory movement of seawater across the beach face. Robinson *et al.* (2007b) demonstrated that the non-linear interactions of the tide with a sloping beach boundary generate a tide-averaged (residual) circulation cell whereby seawater infiltrates the beach in the upper intertidal zone and exfiltrates near the low-tide mark (Figure 5.14a – see colour insert following p. 174). This flow pattern is supported by laboratory experiments (Mango *et al.*, 2004) and intertidal subsurface flow measurements (Robinson *et al.*, 2006). Advective salt transport associated with these circulations leads to the formation of an upper saline plume (or upper mixing zone). The upper saline plume and the classical saltwater wedge confine a freshwater discharge "tube", whereby freshwater discharges around the low-tide mark rather than at the shoreline as occurs for non-tidal conditions (Figure 5.14b – see colour insert following p. 174). Robinson *et al.* (2007b) showed that the average transit time for seawater circulating through the upper saline plume may be up to two orders of magnitude less than that for seawater recirculating through the saltwater wedge. Shorter transit times and faster flow rates associated with the tidal circulation cell indicate that the upper saline plume may represent a significantly more active zone for mixing and reaction than the saltwater wedge dispersion zone. Thus the existence of this tide-induced salt–freshwater mixing zone may have a marked influence on the geochemical conditions in a subterranean estuary and its functioning.

The ratio of tidal forcing (tidal amplitude) to inland forcing (fresh groundwater discharge) strongly controls not only the magnitude of tidally driven seawater recirculation, but also the extent of salt–freshwater mixing in a nearshore aquifer (Robinson *et al.*, 2007b). The forcing of fresh groundwater flow balances the tidal forcing, thus limiting the tidal influence on the system. Based on the estuarine analogy, Robinson *et al.* (2007b) demonstrated that subterranean estuaries may be classified, according to their salt–freshwater mixing conditions, as stratified, partially stratified (partially mixed) and well mixed. Well-mixed systems are characterised by strong tidal forcing relative to inland forcing and vice versa for stratified systems. It should be noted that other parameters, including the beach slope, aquifer depth and sediment properties, also influence the subsurface flow and transport processes to varying degrees (Robinson *et al.*, 2007b, 2007c).

Understanding the flow and salt–freshwater mixing mechanisms provides crucial insight into the geochemical processes in a coastal aquifer, as recirculating seawater transports not only salt but also other chemicals from the ocean to the aquifer. Because of the distinct chemical compositions of the recirculating seawater and fresh groundwater, geochemical transitions (zonations) form at the mixing zones (Charette and Sholkovitz, 2002; Spiteri *et al.*, 2006). For example, field measurements collected on Moreton Island, Australia, revealed significant pH and dissolved oxygen (DO) zonations that were strongly linked to the salinity distribution and therefore influenced by the tidal groundwater dynamics (Robinson *et al.*, 2007a) (Figure 5.15 – see colour insert following p. 174). The pH distribution showed zones of high pH (> 7.5) associated with the upper saline plume and saltwater wedge, and zones of low pH associated with the freshwater discharge "tube" and at the boundaries of the upper saline plume. Dissolved oxygen measurements showed a single zone of high oxygen content in the upper intertidal region. This indicates that although recirculating

seawater maintained a high oxygen content, similar to that of the surface water near the infiltration zone (i.e., in the upper intertidal region), oxygen was rapidly depleted as seawater circulated through the aquifer. The significant difference in redox conditions in the saltwater wedge and upper saline plume reflects the distinct geochemical conditions in these two mixing zones. The low levels of DO in the saltwater wedge are linked with the long transit times associated with density-driven convection, which operates through this zone (Slomp and van Cappellen, 2004; Robinson *et al.*, 2007b). These geochemical zonations are expected to influence reactive processes significantly in the nearshore aquifer, and thus the distribution and fate of many reactive contaminants in the system, i.e., metals (Charette and Sholkovitz, 2002; Charette *et al.*, 2005) and nutrients (Slomp and van Cappellen, 2004; Spiteri *et al.*, 2008).

5.4.2 Implications for contaminant transport and transformation

As discussed above, tides significantly affect the flow and salt–freshwater mixing processes, and consequently the geochemical conditions, in a coastal aquifer. To demonstrate the influence of tides on the transport of non-reactive terrestrial contaminants through a nearshore aquifer, Robinson *et al.* (2007b) conducted numerical tracer experiments. The model used to simulate the tide-induced flow and transport processes was similar to that shown in Figure 5.13. A conservative tracer was injected 50 m landward of the shoreline at the water table. The tracer was injected as a pulse over 1 day. The transport of the tracer through the nearshore aquifer without and with tidal forcing (amplitude = 1 m) is shown in Figures 5.16 and 5.17, respectively. In the absence of tidal forcing, the tracer moved seaward along the top of the aquifer and discharged close to the shoreline. With tides present, the tracer was first transported seaward along the top of the aquifer. Just landward of the high-tide mark the tracer moved downwards, migrating around the tide-induced circulation cell and discharging slightly landward of the low tide mark. Here the tracer was transported through the mixing zone associated with the upper saline plume. This is in contrast to the non-tidal conditions, where the tracer was not transported through any salt–freshwater mixing zones prior to discharge.

The simulated total mass flux across the aquifer/ocean interface indicates that, with tides present, the tracer's subsurface residence time increased by approximately 50 days (Figure 5.18a). A reduction in the peak total mass flux suggests that tidal effects also slightly increased the longitudinal spread of the tracer. This results in the total mass discharge occurring over a longer period of time. Furthermore, the exit concentrations were an order of magnitude lower with tides present (Figures 5.18b, 5.18c). The reduction in exit concentrations is caused primarily by mixing of the tracer with the recirculating seawater. This effect may significantly decrease a contaminant's impact on the interstitial beach environment (i.e., flora and fauna) and nearshore coastal waters. It should be noted that the tidal effects demonstrated by this model differ from previous predictions obtained using a simple "box" model (Li *et al.*, 1999) or a one-dimensional transport model (Li *et al.*, 2004). These models showed that tides may cause rapid flushing of the aquifer, resulting in a significantly reduced

Figure 5.16: Transport of a tracer through a coastal aquifer without tidal forcing (amplitude = 0 m, $Q_f = 2.1\ m^2\ day^{-1}$). Black contour lines show non-dimensional tracer concentration (C/C_0) (a) 1 day, (b) 50 days, (c) 100 days and (d) 150 days after the injection. Concentration contour lines have 0.001 interval spacing.

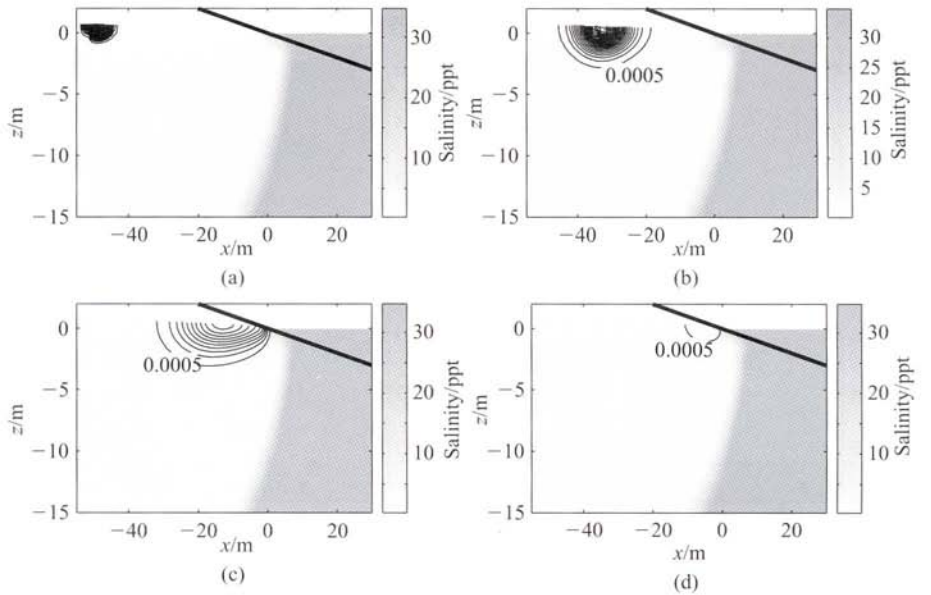

Source: Reprinted from Robinson, C., Li, L. and Barry, D.A. (2007b). Effect of tidal forcing on a subterranean estuary. *Advances in Water Resources*. 30: 851–865. With permission from Elsevier.

tracer residence time and increased chemical transfer to the ocean. The difference in the models' predictions raises questions over the validity of the previous zero- and one-dimensional modelling approaches, and in particular their assumption of well-mixed conditions through the nearshore aquifer.

While Robinson *et al.* (2007b) hypothesised, based on these conservative numerical tracer simulations, that the fate of a reactive contaminant was likely to be affected by geochemical zonations associated with the upper mixing zone, the reactive processes were not simulated. As an extension of this work, with the aim of quantifying the tidal effects on biodegradation, Robinson *et al.* (2009) examined the fate of BTEX (benzene, toluene, ethylbenzene and xylenes) contaminants released in a tidally influenced aquifer. With many industrial areas located in coastal areas, these compounds may find their way into the marine environment via groundwater discharge. Li *et al.* (2004) previously modelled the transport and biodegradation of toluene in a tidally influenced aquifer; however, variable density effects, which significantly influence the physical flow processes, were not considered. Robinson *et al.* (2009) used the coupled density-dependent groundwater flow and multi-species reactive transport code PHWAT (Mao *et al.*, 2006b). A similar model set-up to that of

Figure 5.17: Transport of tracer through a coastal aquifer subject to tidal oscillations (amplitude = 1 m, $Q_f = 2.1\ \mathrm{m\,day^{-1}}$). Black contour lines show non-dimensional tracer concentration (C/C_0) (a) 1 day, (b) 100 days, (c) 140 days and (d) 160 days after the injection. Concentration contours lines have 0.001 interval spacing, and black dashed lines denote the high- and low-tide levels.

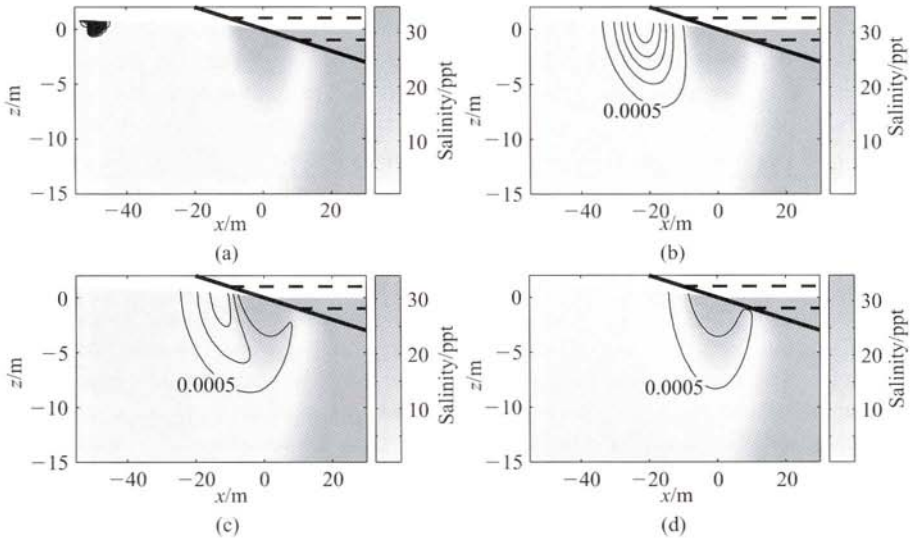

Source: Reprinted from Robinson, C., Li, L. and Barry, D.A. (2007b). Effect of tidal forcing on a subterranean estuary. *Advances in Water Resources*. 30: 851–865. With permission from Elsevier.

Robinson *et al.* (2007b) was adopted. The reactive processes were simulated using an aerobic biodegradation model that considers biomass growth and decay, and also the competitive consumption of oxygen by alternative electron donors such as naturally occurring organic matter and reduced inorganic species (e.g., H_2S, Fe^{2+}, Mn^{2+}). The rate of attenuation of each BTEX compound was described using Monod biodegradation kinetics (Barry *et al.*, 2002).

For the conditions simulated, significant aerobic biodegradation of BTEX was predicted to occur in the oxygenated zone associated with the upper saline plume. This led to a reduction in the total mass of BTEX transported from the aquifer to ocean, and in the rate of chemical discharge. For the base conditions, 79% of toluene initially released in the aquifer was attenuated prior to discharge with tides present, compared with only 1.8% in the absence of tidal forcing. Furthermore, tidal effects were shown to reduce the exit concentrations of all the BTEX compounds considered, except for benzene, to levels below those set by standard international water quality guidelines (e.g., World Health Organization, 2006). Sensitivity analyses showed that enhanced natural attenuation of BTEX compounds is likely at sites where the tidal forcing dominates over the inland forcing (Figure 5.19a). This is because, as discussed previously, the tide counterbalanced by the inland flow controls the magnitude of tide-

Figure 5.18: Effect of tidal forcing on transport of a conservative tracer through a nearshore aquifer. (a) Total flux of tracer across the aquifer/ocean interface versus time after injection for simulation without (solid line) and with (dashed line) tidal forcing, and non-dimensional exit concentrations along the interface (b) without and (c) with tidal forcing. For (b) and (c), results shown are for 100 d (−), 125 days (×), 150 days (○) and 175 days (- -) after the tracer injection. Note the change in scale between (b) and (c).

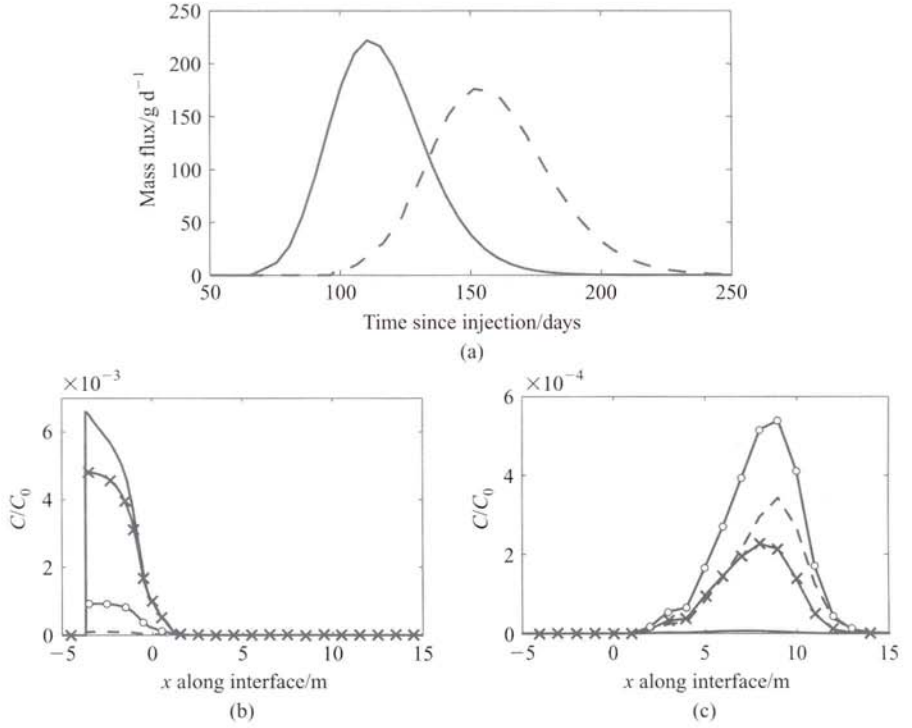

Source: Reprinted from Robinson, C., Li, L. and Barry, D.A. (2007b). Effect of tidal forcing on a subterranean estuary. *Advances in Water Resources*. 30: 851–865. With permission from Elsevier.

induced seawater recirculation and the extent of mixing between seawater and discharging groundwater. In addition, the extent of biodegradation was shown to be limited by the availability of oxygen in the intertidal mixing zone (Figure 5.19b). This availability is controlled by the rate of oxygen input (i.e., rate of seawater recirculation) relative to the rate of natural oxygen-consuming processes in the subsurface. Although in the natural coastal environment both the physical transport and geochemical processes are more complicated than represented by this model, the simulations provide valuable insight into the potential influence of the tide-induced salt–freshwater mixing zone on the fate of terrestrial BTEX compounds discharging to coastal waters via SGD.

Figure 5.19: Influence of (a) tidal amplitude and (b) subsurface oxygen availability on the percentage of toluene injected into an aquifer that is degraded in the subsurface prior to discharge. b_O is a first-order rate constant that describes the consumption of oxygen by natural competing electron donors (i.e., organic matter). As b_O increases, the oxygen availability in the subsurface decreases. The conditions about which parameters are varied are tidal amplitude = 0.75 m, $Q_f = 0.5$ m day^{-1}, aquifer depth = 10 m, beach slope = 0.1, hydraulic conductivity = 15 m day^{-1}, porosity = 0.25, and $b_O = 0.09$ day^{-1}.

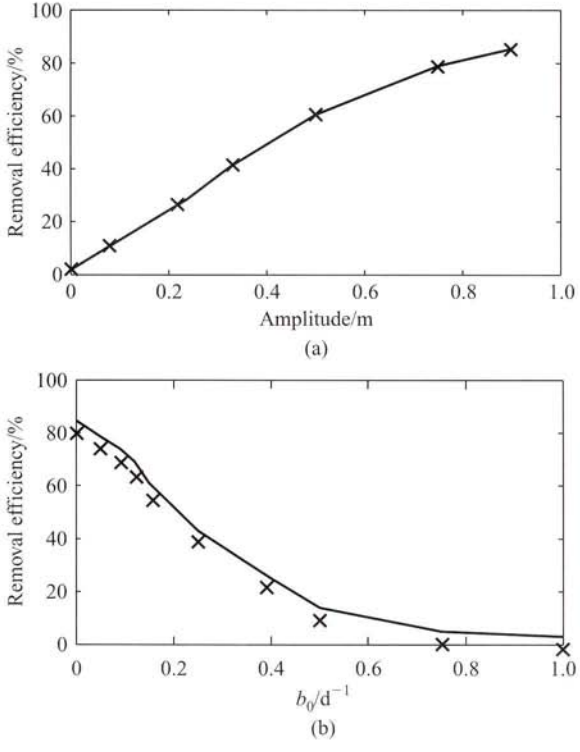

Source: Reprinted from Robinson, C., Brovelli, A., Barry, D.A. and Li, L. (2009). Tidal influence on BTEX biodegradation in sandy coastal aquifers. *Advances in Water Resources*. 32: 16–28. With permission from Elsevier.

5.5 CONCLUDING REMARKS

With environmental impacts increasing, remediation and protection of water resources are and will continue to be important issues. Subsurface water quality affects the well-being of populations worldwide. There are distinct physical characteristics that must be considered in remediation of the subsurface, corresponding to the unsaturated, groundwater and coastal zones. The models presented here account for these characteristics, and permit model-based prediction of the transport and fate of subsurface

contaminants. By capturing the main physical processes involved, as well as incorporating the ability to quantify arbitrary microbial and geochemical processes, environmental engineers can use these models to design, if necessary, optimised remediation schemes.

REFERENCES

Allred, B.J., Bigham, J.M. and Brown, G.O. (2007). The impact of clay mineralogy on nitrate mobility under unsaturated flow conditions. *Vadose Zone Journal*. 6: 221–232.

Amos, R. and Mayer, K. (2006). Investigating the role of gas bubble formation and entrapment in contaminated aquifers: reactive transport modelling. *Journal of Contaminant Hydrology*. 87: 123–154.

Appelo, C.A.J. (1994a). Cation and proton-exchange, pH variations, and carbonate reactions in a freshening aquifer. *Water Resources Research*. 30: 2793–2805.

Appelo, C.A.J. (1994b). Some calculations on multicomponent transport with cation-exchange in aquifers. *Ground Water*. 32: 968–975.

Appelo, C.A.J. and Postma, D. (2005). *Geochemistry, Groundwater and Pollution*, 2nd edn. AA Balkema Publishers, Leiden, The Netherlands.

Ataie-Ashtiani, B., Volker R.E. and Lockington, D.A. (1999). Tidal effects on sea water intrusion in unconfined aquifers. *Journal of Hydrology*. 216: 17–31.

Bajracharya, K. and Barry, D.A. (1995). Analysis of one-dimensional multispecies transport experiments in laboratory soil columns. *Environment International*. 21: 687–691.

Barry, D.A., Starr, J.L., Parlange, J.-Y. and Braddock, R. D. (1983). Numerical analysis of the snowplow effect. *Soil Science Society of America Journal*. 47: 862–868.

Barry, D.A., Bajracharya, K. and Miller, C.T. (1996a). Alternative split-operator approach for solving chemical reaction groundwater transport models. *Advances in Water Resources*. 19: 261–275.

Barry, D.A., Miller, C.T. and Cullingam-Hensley, P.J. (1996b). Temporal discretisation errors in non-iterative split-operator approaches to solving chemical reaction groundwater transport models. *Journal of Contaminant Hydrology*. 22: 1–17.

Barry, D.A., Miller, C.T., Culligan, P.J. and Bajracharya, K. (1997). Analysis of split operator methods for nonlinear and multispecies groundwater chemical transport models. *Mathematics and Computers in Simulation*. 43: 331–341.

Barry, D.A., Bajracharya, K., Crapper, M., Prommer, H. and Cunningham, C.J. (2000). Comparison of split-operator methods for solving coupled chemical non-equilibrium reaction/groundwater transport models. *Mathematics and Computers in Simulation*. 53: 113–127.

Barry, D.A., Prommer, H., Miller, C.T., Engesgaard, P., Brun, A. and Zheng, C. (2002). Modelling the fate of oxidisable organic contaminants in groundwater. *Advances in Water Resources*. 25: 945–983.

Baveye, P., Vandevivere, P., Hoyle, B., DeLeo, P. and Lozada, D.S. (1998). Environmental impact and mechanisms of the biological clogging of saturated soils and aquifer materials. *Environmental Science and Technology*. 28: 123–191.

Biefeldt, A.R., Illangasekare, T., Uttecht, M. and LaPlante, R. (2002). Biodegradation of propylene glycol and associated hydrodynamic effects in sand. *Water Research*. 36: 1707–1714.

Borkovec, M. and Westall, J. (1983). Solution of the Poisson–Boltzmann equation for surface excesses of ions in the diffuse double layer at the oxide electolyte interface. *Journal of Electroanalytical Chemistry*. 150: 325–337.

Boufadel, M.C.A. (2000). Mechanistic study of nonlinear solute transport in a groundwater-surface water system under steady state and transient hydraulic conditions. *Water Resources Research*. 36: 2549–2565.

Breadford, S.A., Šimůnek, J., Bettahar, M., van Genuchten, M.Th. and Yates, S. R. (2003). Modeling

colloid attachment, straining, and exclusion in saturated porous media. *Environmental Science and Technology*. 37: 2242–2250.

Brovelli, A., Malaguerra, F. and Barry, D.A. (2009). Bioclogging in porous media: Model development and sensitivity to initial conditions. *Environmental Modelling and Software*. 24: 611–626.

Charette, M. A. and Sholkovitz, E.R. (2002). Oxidative precipitation of groundwater-derived ferrous iron in the subterranean estuary of a coastal bay. *Geophysical Research Letters*. 29: 1444–1448.

Charette, M.A. and Sholkovitz, E.R. (2006). Trace element cycling in a subterranean estuary, Part 2. Geochemistry of the pore water. *Geochimica et Cosmochimica Acta*. 70: 811–826.

Charette, M.A., Sholkovitz, E.R. and Hansel, C.M. (2005). Trace element cycling in a subterranean estuary, Part 1. Geochemistry of the permeable sediments. *Geochimica et Cosmochimica Acta*. 69: 2095–2109.

Chen, B.F. and Hsu, S.M. (2004). Numerical study of the tidal effects on seawater intrusion in confined and unconfined aquifers by time independent finite difference method. *Journal of Waterway, Port, Coastal and Ocean Engineering*. 130: 191–206.

Church, T. (1996). An underground route for the water cycle. *Nature*. 380: 579–580.

Celia, M.A., Bouloutas, E.T. and Zarba, R.L. (1990). A general mass-conservative numerical solution for the unsaturated flow equation. *Water Resources Research*. 26: 1483–1496.

Clement, T., Hooker, B. and Skeen, R. (1996). Macroscopic models for predicting changes in saturated porous media properties caused by microbial growth. *Ground Water*. 34: 934–942.

Clement, T., Peyton, B., Skeen, R., Jennings, D. and Petersen, J. (1997). Microbial growth and transport in porous media under denitrification conditions: experiments and simulations. *Journal of Contaminant Hydrology*. 24: 269–285.

Cooke, A.J., Rowe, R.K., Rittmann, B.E., VanGulk, J. and Millward, S. (2001). Biofilm growth and mineral precipitation in synthetic leachate columns. *Transport in Porous Media*. 127: 849–856.

Davis, J.A. and Kent, D.B. (1990). Surface complexation modeling in aqueous geochemistry. *In* Hochella, M.F. and White, A.F. (Eds). *Mineral–Water Interface Geochemistry*, Reviews in Mineralogy, Volume 35. Pages 17–260. Mineralogical Society of America, Washington, DC, USA.

Destouni, G. and Prieto, C. (2003). On the possibility for generic modelling of submarine groundwater discharge. *Biogeochemistry*. 66: 171–186.

Dzombak, D.A. and Morel, F.M.M. (1990). *Surface Complexation Modeling: Hydrous Ferric Oxide*. Wiley, New York, USA.

Gaines, G.L. and Thomas, H.C. (1953). Adsorption studies on clay minerals, 2. A formulation of the thermodynamics of exchange adsorption, *Journal of Chemical Physics*. 21: 714–718.

Gapon, Y.N. (1933). Theory of exchange adsorption V. *Russian Journal of General Chemistry*. 3: 667–669.

Ghyben, W.B. (1899). *Nota in verband met voorgenomen put boring Nabji Amsterdam*. Pages 8–22. Tijdschrift van let koninklijk Institut van Ingeniers, The Hague, Netherlands.

Harvey, R. and Garabedian, S. (1991). Use of colloid filtration theory in modeling movement of bacteria through a contaminated sandy aquifer. *Environmental Science and Technology*. 25: 178–185.

Heng, L.K., Tillman, R.W. and White, R.E. (1999a). Anion and cation leaching through large undisturbed soil cores under different flow regimes, 1. Experimental results. *Australian Journal of Soil Research*. 37: 711–726.

Heng, L.K., White, R.E. and Tillman, R.W. (1999b). Anion and cation leaching through large undisturbed soil cores under different flow regimes, 2. Simulation results. *Australian Journal of Soil Research*. 37: 727–741.

Herzberg, A. (1901). Die wasserversorgung einiger Nordseebder. *Zeitshriftfur Gasbeleuchtung und Wasserversorgung*. 44: 815–819.

Hiemstra, T. and Van Riemsdijk, W.H. (1996). A surface structural approach to ion adsorption: the charge distribution (CD) model. *Journal of Colloid and Interface Science*. 179: 488–508.

Hiemstra, T. and Van Riemsdijk, W.H. (1999) Surface structural ion adsorption modeling of competitive binding of oxyanions by metal (hydr)oxides. *Journal of Colloid and Interface Science*. 210: 182–193.

Islam, J., Singal, N. and O'Sullivan, M. (2001). Modeling biogeochemical processes in leachate-contaminated soils: a review. *Transport in Porous Media*. 43: 407–440.

Ives, K. and Pienvichitr, V. (1965). Kinetics of the filtration of dilute suspensions. *Chemical Engineering Science*. 20: 965–973.

Johannes, R.E. (1980). The ecological significance of the submarine discharge of groundwater. *Marine Ecology: Progress Series*. 3: 365–373.

Kanney, J.F., Miller, C.T. and Barry, D.A. (2003). Comparison of fully coupled approaches for approximating nonlinear transport and reaction problems. *Advances in Water Resources*. 26: 353–372.

Kalin, R. (2004). Engineered passive bioreactive barriers: risk-managing the legacy of industrial soil and groundwater pollution. *Current Opinions in Microbiology*. 7: 227–238.

Kildsgaard, J. and Engesgaard, P. (2001). Numerical analysis of biological clogging in two-dimensional sand box experiments. *Journal of Contaminant Hydrology*. 50: 261–285.

Kindred, J. and Celia, M.A. (1989). Contaminant transport and biodegradation, 2. Conceptual model and test simulation. *Water Resources Research*, 25: 1149–1160.

Kinniburgh, D.G., van Riemsdijk, W.H., Koopal, L.K., Borkovec, M., Benedetti, M.F. and Avena, M.J. (1999). Ion binding to natural organic matter: competition, heterogeneity, stoichiometry and thermodynamic consistency. *Colloids and Surfaces A: Physicochemical and Engineering Aspects*. 151: 147–166.

Kirkland, M.R., Hills, R.G. and Wierenga, P.J. (1992). Algorithms for solving Richards' equation for variably saturated soils. *Water Resources Research*. 28: 2049–2058.

Klute, A. (1952). A numerical method for solving the flow equation for water in unsaturated materials. *Soil Science*. 73: 105–116.

Knapp, R., Civan, F. and McInerney, M. (1988). Modeling growth and transport of microorganisms in porous formations. *In* Vichnevetsky, R., Borne, P. and Vignes, J. (Eds). *12th IMACS World Congress on Scientific Computation*. Pages 676–679. Paris, France.

Langevin, C.D., Shoemaker, W.B. and Guo, W. (2003). *MODFLOW-2000, The US Geological Survey Modular Ground-Water model: Documentation of the SEAWAT-2000 Version with the Variable Density Flow Process (VDF), and the Integrated MT3DMS Transport Process (IMT), US Geological Survey*. Open File Report 03-426, Tallahassee, FL, USA, 43 pp.

Lapointe, B.E. and O'Connell, J.D. (1989). Nutrient-enhanced growth of *Cladophora prolifera* in Harrington Sound, Bermuda: eutrophication of a confined, phosphorus-limited marine ecosystem. *Estuarine Coastal Shelf Science*. 28: 347–360.

LaRoche, J., Nuzzi, R., Waters, R., Wyman, K., Falkowski, P.G. and Wallace, D. (1997). Brown tide blooms in Long Island's coastal waters linked to interannual variability in groundwater flow. *Global Change Biology*. 3: 397–410.

Li, L., Barry, D.A. and Pattiaratchi, C.B. (1997). Numerical modelling of tide induced beach water table fluctuations. *Coastal Engineering*. 30: 105–123.

Li, L., Barry, D.A., Stagnitti, F. and Parlange, J.-Y. (1999). Submarine groundwater discharge and associated chemical input to a coastal sea. *Water Resources Research*. 35: 3253–3259.

Li, L., Barry, D.A., Jeng, D.S. and Prommer, H. (2004). Tidal dynamics of groundwater flow and contaminant transport in coastal aquifers. *In* Cheng, A.H.D. and Ouazar, D. (Eds). *Coastal Aquifer Management, Monitoring, Modelling and Case Studies*. Pages 115–141. Lewis Publishers, Boca Raton, Florida, USA.

Lichtner, P.C. (1985). Continuum model for simultaneous chemical reactions and mass transport in hydrothermal systems. *Geochimica et Cosmochimica Acta*. 49: 779–800.

Lichtner, P.C. (1997). Continuum formulation of multicomponent-multiphase reactive transport. *In* Lichtner, P.C., Steefel, C.I. and Oelkers, E.H. (Eds). *Reactive Transport in Porous Media*. Reviews in Mineralogy. Volume 34. Pages 82–129. Mineralogical Society of America, Washington, DC, USA.

Mangold, D.C. and Tsang, C.F. (1991). A summary of subsurface hydrological and hydrochemical models. *Reviews of Geophysics*. 29: 51–79.

Mansell, R.S., Bond, W.J. and Bloom, S.A. (1993) Simulating cation transport during water flow in soil: two approaches. *Soil Science Society of America Journal*. 57: 3–9.

Mango, A.J., Schmeeckle, M.W. and Furbish, D.J. (2004). Tidally induced groundwater circulation in an unconfined coastal aquifer modeled with a Hele-Shaw cell. *Geology*. 32: 233–236.

Mao, X., Enot, P., Barry, D.A., Li, L., Binley, A. and Jeng, D.S. (2006a). Tidal influence on behaviour of a coastal aquifer adjacent to a low-relief estuary. *Journal of Hydrology*. 327: 110–127.

Mao, X., Prommer, H., Barry, D.A., Langevin, C.D., Panteleit, B. and Li, L. (2006b). Three-dimensional model for multi-component reactive transport with variable density groundwater flow. *Environmental Modelling and Software*. 21: 615–628.

Miller, C.T. and Kelley, C.T. (1994). A comparison of strongly-convergent solution schemes for sharp-front infiltration problems. *Computational Methods in Water Resources X*. 12: 325–332.

Miller, C.T., Christakos, G., Imhof, P.T., McBride, J.F., Pedit, J.A. and Trangenstein, J.A. (1998). Multiphase flow and transport modeling in heterogeneous porous media: challenges and approaches. *Advances in Water Resources*. 21: 77–120.

Mualem, Y. (1976). New model for predicting hydraulic conductivity of unsaturated porous media. *Water Resources Research*. 12: 513–522.

Moore, W.S. (1996). Large groundwater inputs to coastal waters revealed by ^{226}Ra enrichments. *Nature*. 380: 612–614.

Moore, W.S. (1999). The subterranean estuary: a reaction zone of ground water and sea water. *Marine Chemistry*. 65: 111–125.

Nielsen, P. (1990). Tidal dynamics of the water table in beaches. *Water Resources Research*. 26: 2127–2134.

Okubo, T. and Matsumoto, J. (1979). Effect of infiltration rate in biological clogging and water quality changes during artificial recharge. *Water Resources Research*. 15: 1536–1542.

Parlange, J.-Y., Stagnitti, F., Starr, J. L. and Braddock, R.D. (1984). Free surface flow in porous media and periodic solution of shallow-flow approximation. *Journal of Hydrology*. 70: 251–263.

Parkhurst, D.L. and Appelo, C.A.J. (1999). *User's Guide to PHREEQC (Version 2), A Computer Program for Speciation, Batch-Reaction, One-Dimensional Transport, and Inverse Geochemical Calculations*. Water Resources Investigations Report 99-4259, USGS, Denver, Colorado, USA, 312 pp.

Philip, J.R. (1969). Theory of infiltration. *Advances in Hydroscience*. 5: 215–296.

Philip, J.R. (1989). The scattering analog for infiltration in porous media. *Reviews of Geophysics*. 27: 431–448.

Pitzer, K.S. (1979). Theory: ion interaction approach. *In* Pytkowicz, R.M. (Ed.). *Activity Coefficients in Electrolyte Solutions*. Pages 157–208. CRC Press, Boca Raton, Florida, USA.

Prieto, C. and Destouni, G. (2005). Quantifying hydrological and tidal influences on groundwater discharges to coastal waters. *Water Resources Research*. 41: W12427.

Prommer, H. and Barry, D.A. (2005). Modeling bioremediation of contaminated groundwater. *In* Atlas, R. and Philp, J.C. (Eds). *Bioremediation: Applied Microbial Solutions for Real-World Environmental Clean-Up*. Pages 108–138. American Society for Microbiology Press, Washington, DC, USA.

Pullan, A.J. (1990). The quasilinear approximation for unsaturated porous media flow. *Water Resources Research*. 26: 1219–1234.

Raats, P.A.C. (2001). Developments in soil-water physics since the mid 1960s. *Geoderma*. 100: 355–387.

Raubenheimer, B., Guza, R.T. and Elgar, S. (1999). Watertable fluctuations in a sandy ocean beach. *Water Resources Research*. 35: 2313–2320.

Reddi, L., Ming, X., Hajra, M. and Lee, I. (2000). Permeability reduction of soil filters due to physical clogging. *Journal of Geotechnical and Geoenvironmental Engineering*. 126: 236–246.

Reilly, T.E. and Goodman, A.S. (1985). Quantitative analysis of saltwater–freshwater relationships in groundwater systems – a historical perspective. *Journal of Hydrology*. 80: 125–160.

Rietra, R.P.J.J., Hiemstra, T. and Van Riemsdijk, W.H. (1999). Sulfate adsorption on goethite. *Journal of Colloid and Interface Science*. 218: 511–521.

Riedl, R.J. and Machan, R. (1972). Hydrodynamic patterns in lotic intertidal sands and their bioclimatological implications. *Marine Biology*. 13: 179–209.

Rittmann, B. (1982). The effect of shear stress on biofilm loss rate. *Biotechnology and Bioengineering*. 24: 501–506.

Robinson, C., Gibbes, B. and Li, L. (2006). Driving mechanisms for flow and salt transport in a subterranean estuary. *Geophysical Research Letters*. 33: L03402.

Robinson, C., Gibbes, B., Carey, H. and Li, L. (2007a). Salt–freshwater dynamics in a subterranean estuary over a spring–neap tidal cycle. *Journal of Geophysical Research*. 112. C09007. doi: 10.1029/2006JC003888.

Robinson, C., Li, L. and Barry, D.A. (2007b). Effect of tidal forcing on a subterranean estuary. *Advances in Water Resources*. 30: 851–865.

Robinson, C., Li, L. and Prommer, H. (2007c). Tide-induced recirculation across the aquifer-ocean interface. *Water Resources Research*. 43: W07428.

Robinson, C., Brovelli, A., Barry, D.A. and Li, L. (2009). Tidal influence on BTEX biodegradation in sandy coastal aquifers. *Advances in Water Resources*. 32: 16–28.

Robinson, M.A., Gallagher, D. and Reay, W. (1998). Field observations of tidal and seasonal variations in groundwater discharge to tidal estuarine surface water. *Ground Water Monitoring and Remediation*. 18: 83–92.

Ross, P.J. (1990). Efficient numerical methods for infiltration using Richards' equation. *Water Resources Research*. 26: 279–290.

Ross, P.J. and Bristow, K.L. (1990). Simulating water movement in layered and gradational soils using the Kirchhoff transform. *Soil Science Society of America Journal*. 54: 1519–1524.

Rowe, R., Armstrong, M. and Cullimore, D. (2000). Particle size and clogging of granular media permeated with leachate. *Journal of Geotechnical and Geoenvironmental Engineering*. 126: 775–786.

Sahimi, M. (1995). *Flow and Transport in Porous Media and Fractured Rock*. VCH Verlagsgesellschaft, Weinheim, Germany.

Scheibe, T., Dong, H. and Xie, Y. (2007). Correlation between bacterial attachment rate coefficients and hydraulic conductivity and its effect on field-scale bacterial transport. *Advances in Water Resources*. 30: 1571–1582.

Seki, K., Thullner, M., Hanada, J. and Miyazaki, T. (2006). Moderate bioclogging leading to preferential flow paths in biobarriers. *Ground Water Monitoring and Remediation*. 26: 68–76.

Simmons, G.M. (1992). Importance of submarine groundwater discharge (SGWD), and seawater cycling to material flux across the sediment/water interfaces in marine environments. *Marine Ecology Progress Series*. 84: 173–184.

Šimůnek, J., van Genuchten, M.T. and Sejna, M. (2005). *HYDRUS-1D Software Package for Simulating the One-Dimensional Movement of Water, Heat and Multiple Solutes in Variably-Saturated Media*, version 3.0, HYDRUS Software Series 1. Department of Environmental Sciences, University of California Riverside, Riverside, CA, USA.

Slomp, C.P. and van Cappellen, P. (2004). Nutrient inputs to the coastal ocean through submarine groundwater discharge: controls and potential impact. *Journal of Hydrology*. 295: 64–86.

Smiles, D.E. and McOrist, G.D. (2001). Radionuclide movement during unsteady, unsaturated soil water flow. *In* Hart, K.P. and Lumpkin, G.R. (Eds). *Scientific Basis for Nuclear Waste Management XXIV*. Materials Research Society Symposium Proceedings, Warrendale, USA, 663, pp. 1117–1123.

Smith, A.J. (2004). Mixed convection and density-dependent seawater circulation in coastal aquifers. *Water Resources Research*. 40: W08309.

Spanier, J. and Oldham, K.B. (1987). *An Atlas of Functions*. Springer, Berlin, Germany.

Spiteri, C. Regnier, P., Slomp, C.P. and Charette, M.A. (2006). pH-dependent iron oxide precipitation in a subterranean estuary. *Journal of Geochemical Exploration*. 88: 399–403.

Spiteri, C., Slomp, C., Tuncay, K. and Meile, C. (2008). Modeling biogeochemical processes in

subterranean estuaries: effect of flow dynamics and redox conditions on submarine groundwater discharge of nutrients. *Water Resources Research*. 44: W04701.

Steefel, C. I. and Lasaga, A.C. (1994). A coupled model for transport of multiple chemical species and kinetic precipitation dissolution reactions with application to reactive flow in single-phase hydrothermal systems. *American Journal of Science*. 294: 529–592.

Stumm, W. and Morgan, J.J. (1996). *Aquatic Chemistry. Chemical Equilibria and Rates*. Wiley, New York, USA.

Taniguchi, M., Ishitobi, T., and Shimada, J. (2006). Dynamics of submarine groundwater discharge and fresh-seawater interface. *Journal of Geophysical Research: Oceans*. 111(C1), C01008.

Taylor, S.W. and Jaffé, P.R. (1990). Biofilm growth and the related changes in the physical properties of a porous medium, 3. Dispersivity and model verification. *Water Resources Research*. 26: 2171–2180.

Thullner, M., Schroth, M.H., Zeyer. J. and Kinzelbach, W. (2004). Modeling of a microbial growth experiment with bioclogging in a two-dimensional saturated porous media flow field. *Journal of Contaminant Hydrology*. 70: 37–62.

Thullner, M., Zeyer, J. and Kinzelbach, W. (2002). Influence of microbial growth on hydraulic properties of pore networks. *Transport in Porous Media*. 49: 99–122.

Tien, C., Turian, R. and Pandse, H. (1979). Simulation of the dynamics of deep-bed filters. *American Institute of Chemical Engineers Journal*. 25: 385–395.

Tipping, E. and Hurley, M.A. (1992). A unifying model of cation binding by humic substances. *Geochimica et Cosmochimica Acta*. 56: 3627–3641.

Tocci, M.D., Kelley, C.T. and Miller, C.T. (1997). Accurate and economical solution of the pressure-head form of Richards' equation by the method of lines. *Advances in Water Resources*. 20: 1–14.

Truesdell, A.H. and Jones, B.F. (1974). WATEQ: a computer program for calculating chemical equilibria of natural waters. *Journal of Research, US Geological Survey*. 2: 233–274.

Tufenkji, N. (2007). Modeling microbial transport in porous media: traditional approaches and recent developments. *Advances in Water Research*. 30: 1455–1469.

Valiela, I., Costa, J., Foreman, K., Teal, J.M., Howes, B. and Aubery, D. (1990). Transport of groundwater-borne nutrients from watersheds and their effects on coastal waters. *Biogeochemistry*. 10: 177–197.

Valiela, I., Foreman, K., LaMontagne, M., Hersh, D., Costa, J., Peckol, P., DeMea-Andreson, B., D'Avanzo, C., Babione, M., Sham, C., Brawley, J. and Lajtha, K. (1992). Coupling of watersheds and coastal waters: sources and consequences of nutrient enrichment in Waquoit Bay, Massachusetts. *Estuaries*. 15: 443–457.

van Genuchten, M.T. (1980). Closed-form equation for predicting the hydraulic conductivity of unsaturated soils. *Soil Science Society of America Journal*. 44: 892–898.

Vandenbohede, A. and Lebbe, L. (2005). Occurrence of salt water above fresh water in dynamic equilibrium in a coastal groundwater flow system near De Panne, Belgium. *Hydrogeology Journal*. 14: 462–472.

Vandevivere, P., Baveye, P., Lozada, D. and DeLeo, P. (1995). Microbial clogging of saturated soils and aquifer materials: evaluation of mathematical models. *Water Resources Research*. 31: 2173–2180.

VanGulck, J.F. and Rowe, R. (2004). Evolution of clog formation with time in columns permeated with synthetic landfill leachate. *Journal of Contaminant Hydrology*. 75: 115–139.

Vanselow, A.P. (1932). Equilibria of the base-exchange reactions of bentonites, permutites, soil colloids, and zeolites. *Soil Science*. 33: 95–113.

Werner, A.D. and Lockington, D.A. (2006). Tidal impacts on riparian salinities near estuaries. *Journal of Hydrology*. 328: 511–522.

Wilson, A.M. (2005). Fresh and saline groundwater discharge to the ocean: a regional perspective. *Water Resources Research*. 41: W02016.

Wissmeier, L. and Barry, D.A. (2008). Reactive transport in unsaturated soil: comprehensive modelling of the dynamic spatial and temporal mass balance of water and chemical components. *Advances in Water Resources*. 31: 858–875.

World Health Organization (2006). *Guidelines for Drinking-Water Quality: Recommendations*. WHO Press, Geneva, Switzerland.

Xie, M.L., Bauer, S., Kolditz, O., Nowak, T. and Shao, H. (2006). Numerical simulation of reactive processes in an experiment with partially saturated bentonite. *Journal of Contaminant Hydrology*. 83: 122–147.

Yeh, G.T. and Tripathi, V.S. (1989). A critical evaluation of recent developments in hydrogeochemical transport models of reactive multichemical components. *Water Resources Research*. 25: 93–108.

Yeh, G.T. and Tripathi, V.S. (1991). A model for simulating transport of reactive multispecies components: model development and demonstration. *Water Resources Research*. 27: 3075–3094.

Zhang, Q., Volker, R.E. and Lockington, D.A. (2001). Influence of seaward boundary condition on contaminant transport in unconfined coastal aquifers. *Journal of Contaminant Hydrology*. 49: 201–215.

Zheng, C. and Bennett, G.D. (2002). *Applied Contaminant Transport Modeling*, 2nd edn. John Wiley & Sons, New York, USA.

Zysset, A., Stauffer, F. and Dracos, T. (1994). Modeling of reactive groundwater transport governed by biodegradation. *Water Resources Research*. 30: 2423–2434.